Convergent neural signatures of speech prediction error are a biological marker for spoken word recognition

Ediz Sohoglu[1], Loes Beckers[2,3,4] and Matthew H. Davis[2]

1) School of Psychology, University of Sussex, Brighton, UK
2) MRC Cognition and Brain Sciences Unit, Cambridge, UK
3) Department of Otorhinolaryngology, Donders Institute for Brain, Cognition and Behaviour, Radboud University Medical Center, Nijmegen, Netherlands
4) Cochlear Ltd., Mechelen, Belgium

Keywords: Predictive coding, Speech perception, MEG, fMRI

Acknowledgements: This research was supported by intermural funding from the Medical Research Council to the Cognition and Brain Sciences Unit (MC_UU_0005/5 and MC_UU_00030/6 to M.H.D.). We thank Sander Van Bree and Clare Cook for assistance with MEG data collection and Steve Eldridge and Karen Kabakulu for assistance with radiography.

Address correspondence to:

Ediz Sohoglu (E.Sohoglu@sussex.ac.uk) or Matthew Davis (matt.davis@mrc-cbu.cam.ac.uk)

Abstract

We used MEG and fMRI to determine how predictions are combined with speech input in superior temporal cortex. We compared neural responses to bisyllabic spoken words in which the first syllable strongly or weakly predicts the form of the second syllable (e.g. “bingo” versus “tango”). We further compared neural responses to the same second syllables when heard in an unfamiliar pseudoword and therefore in a situation in which predictions mismatch with sensory input (e.g. “snigo” and “meago”). Across multiple imaging modalities and analysis approaches (including information-based pattern analysis methods), we show that neural representations of second syllables are suppressed by strong predictions when predictions match sensory input. However, neural representations of the same second syllables show the opposite effect (i.e. enhanced representations following strongly than weakly-predicting syllables) when predictions mismatch with sensory input. Computational simulations show that this interaction between prediction strength and (mis)match is consistent with prediction error but not alternative (sharpened signal) computations. Neural signatures of prediction error are observed early (beginning 200 ms after the onset of the second syllable), localise to early auditory regions (in fMRI, bilateral Heschl’s gyrus and STG) and are expressed as changes in low-frequency (theta and alpha) power. Finally, we show that even a non-speech noise that replaces a predicted second syllable can evoke informative neural activity patterns, consistent with negative prediction errors. Our study therefore provides convergent neural evidence that speech perception is supported by the computation of prediction errors in auditory brain regions. These prediction error computations play a central role in the identification of familiar spoken words and perception of unfamiliar pseudowords.

Introduction

The information reaching our senses is incomplete and ambiguous such that perception requires active computations for successful interpretation. Nowhere is this more evident than with speech perception. To paraphrase Heraclitus, “No listener ever hears the same speech twice, for it’s not the same sounds and they’re not the same listener”. No two productions of the same word are ever acoustically identical; each will be differently realised due to the ubiquitous variability of natural speech produced by different talkers, and in different contexts. No listener is ever the same as they will have different expectations or prior knowledge for the speech they will hear at different times. Consider for example, hearing a word starting with the syllable “tan”. It can be unclear whether this is the start of the word “tangle”, “tango” or another word that starts with the same initial sounds. This ambiguity can be present even if speech is clearly heard in a quiet background. Yet when listening during everyday conversation, our subjective impression is that spoken word recognition is immediate, clear and accurate. How do listeners achieve such reliable perception despite transient sensory ambiguity?

In answering this question, the notion of Bayesian inference is commonly invoked. That is, listeners combine sensory evidence with prior knowledge about which speech sounds they will hear [1]. This proposal is appealing because it can explain how listeners process speech both rapidly and accurately [2,3]. However, despite widely held agreement that listeners use prior knowledge during speech processing, it remains unclear how this is implemented neurally. One possibility is that neural representations of speech are enhanced by prior knowledge [4]. This has been termed the sharpened signal account [5–7] because in this proposal, neural responses to expected stimuli come to resemble a sharpened (i.e. less ambiguous or less noisy) version of the sensory input. However, it is also the case that expected speech sounds carry relatively little information. Therefore, an alternative and potentially more efficient strategy would be to compute prediction errors i.e. the difference between heard and predicted sounds [8–11]. In this prediction error account, neural representations are suppressed by prior knowledge and unexpected (and therefore novel and unexplained) sensory information is prioritised for processing.

Sharpened signal and prediction error accounts have been difficult to distinguish experimentally. This is because in both accounts, prior knowledge has a similar effect on the overall strength of neural responses [5,6]. In the case of the prediction error account, brain responses tuned to the heard stimulus features are suppressed when those stimulus features are expected, resulting in an overall reduction in brain activity. With the sharpened signal account, although brain responses tuned to the heard stimulus features are enhanced, this is accompanied by the suppression of responses tuned away from the stimulus input features i.e. competing interpretations. This suppression of brain responses tuned away from the input features also leads to overall weaker activity. Therefore, previous findings that neural responses correlate with moment-by-moment phoneme and word predictability during story comprehension [12–15] do not provide unambiguous support for prediction error over sharpened signal accounts. Some accounts have proposed that sharpening and prediction error computations operate in parallel [8], and localise to different cortical layers [16]. Nonetheless, we focus on contrasting sharpening and prediction error mechanisms since single mechanism accounts have been proposed in speech perception [4,17,18] and remain to be distinguished [19].

Neural pattern analysis methods that permit measurement of the information conveyed by neural responses can distinguish between sharpened signal and prediction error computations. Indeed, previous work using fMRI [17] and MEG [20] has demonstrated a distinctive neural marker of prediction errors which is that neural representations of sensory features of speech show an interaction between signal quality and prior knowledge. This interaction arises because sensory signals that match strong prior expectations are explained away more effectively as signal quality increases and hence neural representations are suppressed even as perceptual outcomes improve. Whereas for sensory signals that follow less informative prior knowledge, increased signal quality leads to a corresponding increase in sensory information that remains unexplained. By contrast, under a sharpened signal account, computational simulations show that neural representations (like perceptual outcomes) are similarly enhanced by increased signal quality and prior knowledge [17,20]. Therefore, by experimentally manipulating both signal quality and prior knowledge, and observing the consequences on pattern-based neural measures, it is possible to distinguish between accounts.

However, in the aforementioned studies [17,20], listeners heard highly distorted (and unnatural sounding) spoken words while prior knowledge was manipulated by presenting matching or nonmatching written words before speech was heard. This is far removed from real-world conditions in which speech is clearly heard (non-distorted) and predictions are not derived from external written cues but from linguistic knowledge e.g. word probabilities vary based on usage frequency and preceding sentence context. Indeed, some investigators have argued that previously documented effects of prior knowledge or prediction on language processing are the consequence of "prediction encouraging" paradigms and fail to generalise to settings more representative of real-world perception [21].

In the current study, we return to this issue by presenting listeners with clearly spoken words. We experimentally manipulated the strength and accuracy of listeners' prior knowledge with the goal of adjudicating between sharpened signal and prediction error accounts. Here our manipulation of prior knowledge is based on information intrinsic to the speech signal and arises from listeners' long-term linguistic knowledge of the sounds of familiar spoken words. We compare neural responses to bisyllabic spoken words (e.g. "bingo", "tango") in which the first syllable strongly (in "bingo") or weakly (in "tango") predicts the form of the second syllable (Figure 1A). In addition, we compare neural responses to the same second syllables when heard in a pseudoword context (e.g. "snigo", "meago"). Pseudowords, by definition, are unfamiliar to participants and therefore the second syllable of these items mismatches with listeners' predictions. This creates a listening situation in which strong predictions entirely mismatch with sensory input. This cannot be observed in other experimental situations that forego manipulation of speech content (e.g. story comprehension) and creates a further opportunity for adjudicating between sharpened signal and prediction error computations.

We first performed computational simulations (using model architectures and representations schematised in Figure 1B, C) to show that, as intended, our experimental manipulations of prediction strength and match/mismatch result in dissociable effects for sharpened signal and prediction error computations (Figure 1D, E). While prediction strength and prediction congruency act to enhance sharpened signal representations, prediction error computations show an interaction between prediction strength and congruency. This interaction is driven by a reduction of prediction errors when strong predictions match the sensory input compared with

weak predictions. When predictions mismatch with sensory input, however, the opposite occurs with prediction errors slightly increasing with prediction strength. We then measured neural responses using 204-channel MEG and 3T fMRI in separate groups of listeners while they performed an incidental (pause detection) listening task to maintain attention (Figure S1A). Across multiple imaging modalities (MEG, fMRI), analysis approaches (signal magnitude and pattern), and signal domains (time and time-frequency), we provide convergent neural evidence that speech perception is supported by the computation of prediction errors in auditory brain regions.

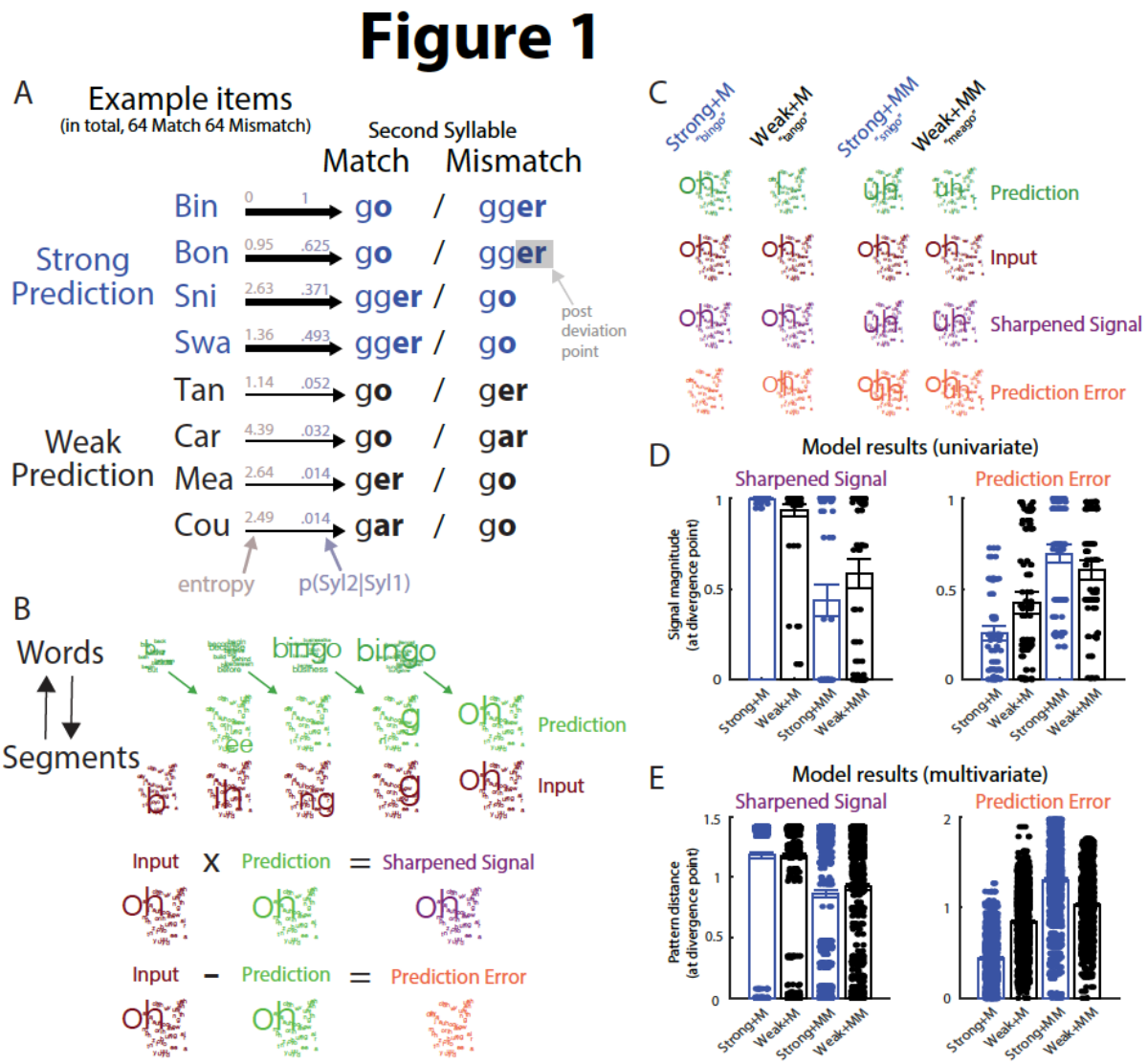

Figure 1- (A) Our stimuli consisted of multiple sets of bi-syllabic spoken words ("bingo", "bongo", etc.) and pseudowords ("bingger", "bongger"). Note that the acoustic-phonetic form of the syllables spelled "ger", "gger" and "gar" in "Snigger", "Swagger", "Meager" and "Cougar" are identical in our stimuli (transcribed /g@r/). We show their more familiar orthographic form for illustration purposes only. Purple numbers indicate the strength of

predictions for the second syllable of each item, operationalized as p(Syl2|Syl1): the probability of hearing the second syllable, conditioned on the first syllable. Brown numbers indicate the entropy of predictions over all possible syllables (equivalent to the weighted average of surprisal over syllables [22]). Thickness of arrows depicts the overall higher p(Syl2|Syl1) and lower entropy for Strong vs Weak Prediction items. By cross-splicing the syllables in our word items, we created a set of pseudowords in which predictions mismatched with Syl2. The earliest speech segment when the words diverged from the pseudowords (the divergence point) is indicated in bold and always occurred at the second segment of Syl2. (B) Model representations for the example word "bingo", visualized using word and segment clouds with larger text indicating higher probabilities. Word level representations show posterior probabilities for each word as each segment in the input word is heard prior to the deviation point (the ten words with the highest probabilities at any one timepoint are shown for illustration purposes). Word posteriors provide predictions for which segment will be heard next (segment predictions shown as green colored phonetic transcriptions). Segment predictions are then combined with the sensory evidence ('Input'; shown as brown colored phonetic transcriptions) through sharpened signal (multiplication) or prediction error (subtraction) computations with outcomes depicted on the right as purple and orange segment clouds, respectively (shown only for the deviation point). (C) Example model representations for all four experimental conditions at the deviation point for Strong + Match ("bingo"), Weak + Match ("tango"), Strong + Mismatch ("snigo"), Weak + Mismatch ("meago") items. Due to differential predictions (top-line, green), identical speech input (/oh/, second line, brown), elicits different neural representations for sharpened signal (third line, purple) and prediction error (fourth line, orange) representations. (D) Summary of sharpened signals and prediction error simulations at the divergence point, used to predict the magnitude of neural responses (signal magnitude analysis). Dots indicate the model signals for each individual item (32 items in each condition) with bars and error bars indicating the mean and standard error across the full item set). (E) Summary of simulations used to predict neural pattern distances, shown in the same way as panel D except the individual datapoints and bars depict the dissimilarity between model representations for all pairs of items (496 item pairs, i.e. 32x31/2) within each condition (pattern analysis).

Results

Stimulus properties and behavioural responses

To manipulate listeners' predictions, we chose a set of 64 bisyllabic words in which the first syllable (Syl1) either strongly or weakly predicts the same second syllable (Syl2; see Figure 1A which depicts some example items). Here we operationalise prediction strength as the probability of hearing Syl2, conditioned on Syl1 (p(Syl2|Syl1); see Methods section for details and refs. [2,11,12,22]). For example, after hearing the first syllable "bin", there is only one potential word candidate (*bingo*). Therefore, based on their experience of spoken English, listeners will predict that the second syllable "go" is most likely after hearing "bin" (p(Syl2|Syl1) = 1). In contrast, after hearing the first syllable "tan", there are more potential word

candidates (e.g. *tango, tangle, tanker, tankard, tang*) and of these words, *tango* is less frequently used than the competitors *tangle* and *tang*. As a result, listeners can only make a weak prediction for “go” after hearing “tan” (p(Syl2|Syl1) = .052). We validated our experimental manipulation of prediction strength by asking a separate group of listeners to perform a free report gating task [see ref. ,23 and SI Methods and Results]. This confirmed that listeners were more likely to predict the second syllables of our Strong items than for Weak items. Further validation of our experimental manipulation is provided when assessing listeners’ memory for the pseudowords in a cued recall task (see SI Results).

In addition to manipulating the strength of listeners’ predictions, we manipulated whether Syl2 matched or mismatched with listeners’ predictions. This was achieved by cross-splicing Syl1 and Syl2 between words to create a set of corresponding pseudowords sharing the same set of syllables as the word items. For real word items, Syl2 always matches predictions, at least to some degree. For pseudowords, p(Syl2|Syl1) approaches zero. This is by definition, since these Syl1 and Syl2 combinations will never previously have been heard by participants as English spoken words prior to the experiment. Therefore, for these items, Syl2 entirely mismatches with listeners’ predictions. Note we can still expect an effect of prediction strength for Mismatch items since Strong and Weak items differ not only in terms of p(Syl2|Syl1), but also in entropy over all possible syllables i.e. the overall uncertainty of predictions (see SI Results and Figure S4A). Indeed in natural speech, conditional probabilities for upcoming speech sounds are highly correlated with entropy [12,14,22]. Going back to the *bingo* example above, entropy is relatively low after hearing Syl1 because only one word (*bingo*) can be predicted. For *tango* on the other hand, entropy is relatively high after hearing Syl1 because predictions are spread over more word candidates. Thus, while we constructed our stimuli based on p(Syl2|Syl1), our manipulation of prediction strength reflects differences in both p(Syl2|Syl1) and syllable entropy.

To assess neural responses to these stimuli, we recorded MEG (N=19) and fMRI (N=21) data in two separate groups of listeners (Figure S1A). To maintain listeners’ attention, participants were asked to detect brief (200 ms) pauses inserted between Syl1 and Syl2 in occasional target items. As shown in Figure S1B and S1C, participants could perform this task quickly and accurately (d-prime higher than 3 and with response times on target-present trials less than 1100 ms).

Computational simulations

We performed simulations of sharpened signal and prediction error computations supporting spoken word and pseudoword recognition (model architectures and representations schematised in Figure 1B, C). The underlying mechanisms were derived from established Bayesian models of spoken word recognition [e.g. 2] guided by observations of functionally equivalent but neurally distinct implementations of these. We focus on the timepoint at which the words and pseudowords in our stimuli diverge (the divergence point; highlighted as bold speech segments in Figure 1A). This is the time at which our experimental manipulation of prediction congruency can affect brain responses: in phonemes, this is at the onset of the second speech segment during Syl2 (98 ms after Syl2 onset on average, with a standard deviation of 46 ms).

Both sharpened signal and prediction error computations are derived from conditional (posterior) word probabilities, as estimated using Bayes theorem (for details, see Methods). As with previous work [e.g. 2,11,12], prior speech segment probabilities are estimated from the relative frequencies of the words matching the preceding speech signal, which is appropriate for spoken words heard in isolation (see Methods for details). Our estimates of the sensory evidence are derived from the acoustic similarity between individual speech segments and expresses the degree to which the sensory input matches internal representations of spoken words [2,24]. Because our stimuli consisted of clear speech recordings, we simulated conditions in which the sensory evidence was high (i.e. there was minimal sensory uncertainty; see Methods) but dissociable sharpened signal and prediction error computations are observed when simulating a range of sensory uncertainty levels (Figure S3).

To relate these simulations to observed neural responses, we apply signal magnitude (univariate) and pattern (multivariate) analysis procedures used in our MEG and fMRI analyses (described in a subsequent section) to simulated representations of speech segments at the divergence point (results shown in Figure 1D, E). The pattern analysis (Figure 1E) quantifies how strongly phonetic content in the speech input is represented in sharpened signal and prediction error computations for each of the four experimental conditions (the 2-by-2 crossing of prediction strength and congruency). This is achieved by quantifying the dissimilarity between model

representations (pattern distances) for all pairs of items within each condition. The signal magnitude analyses (Figure 1D), on the other hand, focusses on the overall strength (rather than pattern) of neural responses. For this magnitude analysis, one approach would be to sum model signals over all possible segment representations (48 in total). However, this approach is ill-suited for the sharpened signal simulation since the model representations correspond to posterior probability distributions and hence all simulated signals are normalized to sum to one (and will hence never differ between conditions). For relating to signal magnitude analyses (for both sharpened signal and prediction error simulations), we therefore analysed model representations specifically for the speech segment that will be heard at the divergence point. Note however that this magnitude analysis of simulated representations ignores contributions from responses tuned away from the input stimulus. This is a questionable simplification since observed neural responses are likely to reflect contributions from neurons tuned both to and away from the input stimulus. We present this magnitude analysis for completeness but we consider the pattern analysis to provide the most informative test of sharpening and prediction error accounts since here responses tuned both to and away from the input stimulus are jointly analysed.

The results of our simulations of both signal magnitude (Figure 1D) and pattern analyses (Figure 1E) show that while sharpened signal representations are enhanced for Match items (particularly when predictions are strong), prediction strength and congruency have interactive effects on prediction error representations. Specifically, for signals that match prior predictions, prediction errors decrease in magnitude and pattern distance for stronger predictions. However, the opposite effect occurs when predictions mismatch with predictions; that is prediction error is increased, and more informative for syllables that mismatch with stronger predictions. In addition, prediction errors are overall larger for Mismatch compared with Match items, reflecting the absence of accurate predictions following the divergence point of the pseudoword (Mismatch) stimuli. These simulations therefore confirm that our experimental manipulations can distinguish between sharpened signal and prediction error computations. We can therefore evaluate the extent to which observed brain responses are more consistent with sharpened signal or prediction error computations.

MEG signal magnitude

As shown in Figure 2A, we assessed MEG responses timelocked to the onset of Syl2, with respect to a baseline period prior to Syl1 (i.e. speech onset; see Methods). Note that as a result, the MEG responses at negative latencies shown in Figure 2A are non-zero (coinciding with sensory input from the Syl1 portion of our spoken stimuli).

Before assessing the neural timecourse of between-condition differences, we selected 20 (planar gradiometer) sensors with the strongest responses (signal power averaged over conditions, separately for each hemisphere and participant). Sensor selections (i.e. those sensors with the strongest responses) were distributed over temporal and frontal sites bilaterally (shown inset within Figure 2A), consistent with neural generators in superior temporal cortex. We then summarised MEG responses in these “speech responsive” sensors as the RMS amplitude across sensor selections for each timepoint. Reported effects are all FWE (family-wise error) rate corrected for multiple comparisons across timepoints using cluster permutation methods and a clusterwise threshold of $p < 0.05$.

Following Syl2 onset, prediction strength (Strong vs Weak) and congruency (Match vs Mismatch) had interactive influences on MEG responses from around 200 to 600 ms (results for left hemisphere sensors are shown in Figure 2A; similar results are seen for right hemisphere sensors, depicted in Figure S2A). Stronger predictions resulted in weaker MEG responses but only when speech matched with predictions (significant timepoints for the interaction between prediction strength and congruency are indicated as horizontal cyan bars; the simple effect of Strong vs Weak for Matching items is shown as the grey shaded area between MEG traces). MEG responses also showed a main effect of prediction congruency with overall larger responses for Mismatch vs Match items (significant timepoints shown as red horizontal line). These two patterns – interaction between prediction strength and congruency, together with a main effect of Mismatch > Match – is more consistent with prediction error than sharpened signal computations (compare with Figure 1D). Note that although MEG responses do not increase with prediction strength for mismatching items in this particular analysis, they do for other analyses that will be reported below (a pattern also observed in the simulations of Figure 1D).

Prior to Syl2 onset, a different pattern of results was observed. Here MEG responses increased with prediction strength (indicated as horizontal purple bars in Figure 2A). While the timing of this effect (before Syl2 onset) suggests a neural signal reflecting predictions rather than prediction errors, we cannot rule out that this pre-Syl2 effect reflects acoustic differences since the Syl1 portion of Strong items is longer in duration than for Weak items (see SI Results and Figure S4A). This duration difference could potentially lead to larger MEG signal when timelocking to Syl2 onset as neural responses would be shifted later in time for Strong versus Weak items. Indeed, when timelocking to Syl1 onset to control for this difference in timing, the increased MEG response for Strong versus Weak items is no longer apparent (Figure S2C). Note that these or other acoustic confounds can only affect pre-Syl2 neural responses since our cross-splicing procedure ensures that post-Syl2, there are no acoustic differences between our four conditions (see Figure 1A and Figure S4A). Since representations of Syl2 are critical for distinguishing sharpened signal from prediction error computations (Figure 1D and 1E), we subsequently focus on post-Syl2 effects.

To test whether Syl2 responses are modulated by prediction strength for single items, we correlated p(Syl2|Syl1) with MEG responses across items separately for Match and Mismatch items. We show group-averaged Spearman correlations between prediction strength and MEG responses in left hemisphere sensors in Figure 2B (right hemisphere correlations shown in Figure S2B). Consistent with the previous analysis averaged over items (Figure 2A), following Syl2, there was an interaction between prediction strength and congruency from 168 to 300 ms and from 356 to 460 ms: Stronger predictions that matched with speech were associated with weaker MEG responses and this correlation differed from that observed when predictions mismatched (significant timepoints indicated as horizontal cyan bars). Individually, the correlations within the Matching condition were significantly negative (indicated as the grey shaded area). Within the Mismatching condition, correlations were weakly positive and significant in the right hemisphere at a later latency (Figure S2B, 500-600 ms). Again, this pattern of results is more consistent with prediction error than with sharpened signal computations. Thus, this analysis demonstrates that the item-averaged effects depicted previously in Figure 2A extend to single items. That is, the strength of lexical level predictions modulates neural responses to heard speech. However, the magnitude and direction

of this effect depends on whether subsequent segments match or mismatch with predictions; the significant interaction shown in both factorial and graded analyses is consistent with neural responses being correlated with the magnitude of prediction errors.

To probe time-frequency correlates of prediction strength and congruency, we also assessed changes in spectral power in the 2-48 Hz range. This time-frequency analysis also showed a significant interaction between prediction strength and congruency in the theta band, with a peak frequency at 3 Hz and a peak latency 120 ms after Syl2 onset (left hemisphere results shown in Figure 2D, similar observations in right hemisphere sensors shown in Figure S2D). Similar to the time-domain analyses above, stronger predictions resulted in weaker MEG power but only when speech matched with predictions (see summary in Figure 2C). We also analysed high-frequency gamma activity (52-90 Hz) but did not observe reliable condition-wise differences.

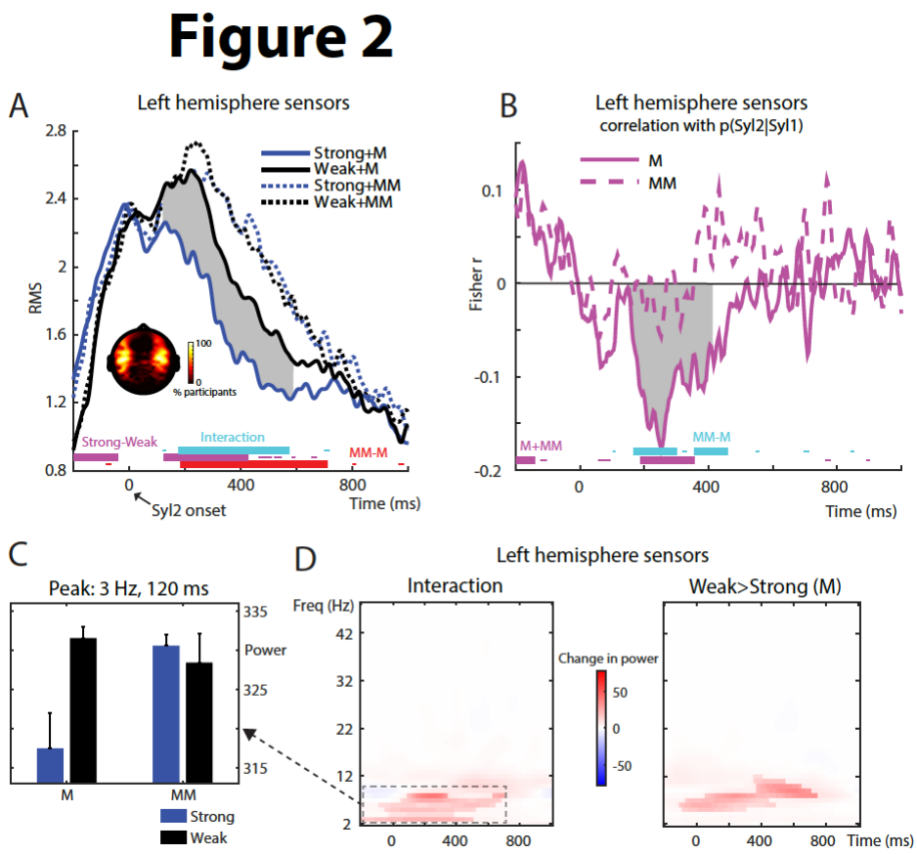

Figure 2- MEG signal magnitude results. (A) Traces indicate the RMS of the MEG signal across "speech-responsive" sensors in the left hemisphere, timelocked to the onset of the second syllable (Syl2). Sensor selections are indicated in the topography as the percentage of participants for which a sensor was selected.

Thick horizontal bars at the bottom of the graph indicate timepoints when statistical contrasts were significant at a clusterwise threshold of p < .05 FWE corrected (thin horizontal bars show significance at an uncorrected p < .05 threshold). Grey shaded area indicates timepoints when the effect of Strong vs Weak in the Match condition was significant at p < .05 (FWE cluster corrected). M = Match. MM = Mismatch. (B) Group-averaged correlations in left hemisphere sensors between p(Syl2|Syl1) and the RMS of the MEG signal. Gray shaded area indicates timepoints when the correlations within Match or Mismatch conditions were significant at p < .05 (FWE cluster corrected). (C) Bar graph indicates group means and within-subject standard errors [25] for the four experimental conditions after averaging MEG power over the temporal and frequency extent of the interaction cluster reported in panel D. (D) Image depicts changes in MEG power (between condition differences) across time and frequency in left hemisphere sensors for the interaction (left panel) and simple effect of Weak > Strong in Match trials (right panel) . Nontransparent colors indicate significance at p < .05 (FWE cluster corrected) while transparent colors show p < .05 (uncorrected). Interaction effect was computed as (Strong-Weak [Mismatch)]) – (Strong-Weak[Match]).

fMRI signal magnitude

In a separate group of listeners, we recorded BOLD functional MRI responses to the same stimuli, using a sparse fMRI sequence so that speech was presented in the silent periods between scans (Figure S1A). The procedure (task and number of stimulus repetitions) was otherwise identical to that used in the MEG experiment. This allowed us to localize the neural generators of the MEG effects reported above. Reported effects are all FWE rate corrected using a clusterwise threshold of p < 0.05.

As shown in Figure 3A, the main effect of Mismatch > Match (that was observed following Syl2 onset with MEG) localized to middle/anterior STG bilaterally (see Table 1 for MNI space coordinates). The main effect of Strong>Weak (observed with MEG prior to Syl2 onset) localized to Heschl's gyrus (HG), extending into STG. Despite observing an interaction between prediction and congruency on MEG responses, there was no equivalent effect in this fMRI analysis. We suggest this is because of the reduced temporal resolution of fMRI, which makes it more difficult to resolve individual responses to Syl2 and Syl1.

A potentially more sensitive analysis is to correlate p(Syl2|Syl1) with the magnitude of the BOLD signal across individual items (equivalent to the MEG analysis shown in Figure 2B). Employing this approach, fMRI responses in bilateral HG and middle STG again increased with prediction strength (positive correlation) for both Match and Mismatch items (shown in Figure 3B with MNI space coordinates listed in Table 1), demonstrating that the effect depicted previously for items that

differ in averaged prediction strength in Figure 3A is also observed for single items which encompass a range of prediction strengths. Importantly, we also observed an interaction between p(Syl2|Syl1) and prediction congruency in right anterior STG (shown in Figure 3B), revealing a potential neural generator of the interaction effects previously observed with MEG (Figure 2B and Figure S2B). Although with fMRI, the effect appears driven by a positive correlation in the Mismatch condition (rather than a negative correlation for Match items), we note that right-hemisphere MEG sensors also show this effect at later latencies (Figure S2B).

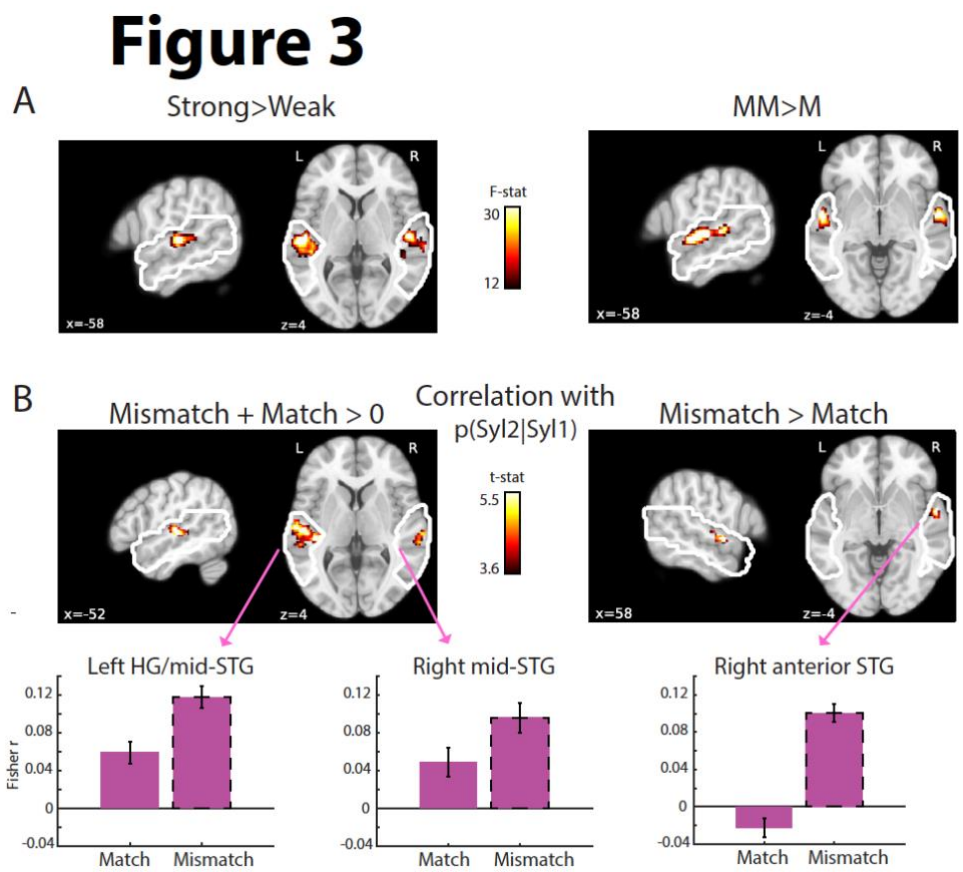

Figure 3 fMRI signal magnitude results. (A) Repeated measures ANOVA showed main effects of prediction strength (left panel) and congruency (right panel). Statistical maps (p < .05 FWE cluster corrected) are shown overlaid onto a template brain in MNI space. White outlines indicate the search volume which included superior and middle temporal regions bilaterally. (B) Statistical maps (p < .05 FWE cluster corrected) for correlations between p(Syl2|Syl1) and BOLD magnitude. In HG extending into middle STG (left panel), correlations are significantly positive and do not differ between Match and Mismatch items (equivalent to a main effect of prediction strength). In anterior STG (right panel), correlations are significantly larger for Mismatch than for Match items. Bar graphs show group-averaged correlations (Fisher-transformed r-values) between conditional probability and BOLD magnitude averaged across voxels in the clusters indicated (arrows). Error bars show within-subject standard errors suitable for statistical comparison between conditions.

Table 1

Location	Extent	Z-stat	x	y	z
Univariate Strong > Weak					
Right Heschl's Gyrus	551	5.74	54	-16	2
Right mid-STG		4.84	64	-14	0
Right mid-STG		4.05	66	-26	4
Left mid-STG	551	5.41	-58	-22	4
Left Heschl's Gyrus		4.55	-44	-24	2
Left mid-STG		4.55	-46	-32	4
Univariate Mismatch > Match					
Left mid-STG	569	6.00	-64	-24	6
Left mid-STG		5.81	-60	-16	2
Left anterior-STG		5.62	-58	-4	-4
Right anterior-STG	205	5.25	58	-4	-4
Right mid-STG		4.51	64	-16	0
Right mid-STG		3.54	56	-14	-2
Univariate Strong+Noise > Weak+Noise					
Left anterior-STG	245	4.42	-54	-12	2
Left Heschl's Gyrus		4.21	-44	-22	-2
Left mid-STG		3.31	-60	-24	2
Right posterior-STG	56	4.25	64	-44	10
Right posterior-MTG		3.58	60	-54	6
Right mid-STG	115	4.00	54	-20	0
Right Heschl's Gyrus		3.30	48	-14	0
Right anterior-STG		3.10	58	-12	-4
Univariate correlations with p(Syl2|Syl1) Mismatch+Match					
Left Heschl's Gyrus	467	5.01	-52	-22	2
Left Heschl's Gyrus		4.85	-42	-28	4
Left mid-STG		4.62	-62	-18	6
Right mid-STG	105	4.04	66	-24	6
Right mid-STG		3.96	64	-32	6
Right mid-STG		3.56	54	-26	0
Univariate correlations with p(Syl2|Syl1) Mismatch>Match					
Right anterior-STG	71	4.58	58	-2	-4
Right anterior-STG		3.81	50	-4	-2
Right anterior-STG		3.59	58	-10	2
Multivariate Syl2 phonetic distance					
Right Heschl's Gyrus	148	4.49	56	-6	2
Left Heschl's Gyrus	146	4.01	-44	-20	0

Table 1- MNI coordinates for fMRI analyses. Also shown are the spatial extent (number of voxels) and peak statistic for each cluster.

MEG pattern analysis

The signal magnitude analyses above shows that the magnitude of neural responses in superior temporal regions is modulated by syllable prediction strength in different directions depending on whether heard speech matches or mismatches with predictions. While the direction of these neural effects is in line with the magnitude of prediction error in our computational simulations, as mentioned above, this magnitude analysis ignores contributions from responses tuned away from the input stimulus. Multivariate analysis of the full representational pattern, which incorporates contributions from responses tuned both to and away the input stimulus, therefore provides the critical test of sharpening and prediction error accounts. Simulations of prediction error computations show that representational

patterns show an interaction between prediction strength and congruency (Figure 1E) which is not shown for sharpened signal computations.

To examine how predictability modulates neural representational patterns in our MEG data, we computed the Euclidean distance between sensor patterns (over the entire 204 array of planar gradiometers) evoked by pairs of items. Taking this approach, we first asked whether the MEG signal contained phonetic information about the syllables by correlating neural pattern distances with the phonetic dissimilarity between the syllables of item pairs (based on a representational dissimilarity matrix derived from the Levenshtein distance between phonetic transcriptions for different syllables, as illustrated in Figure 4A for Syl2 and Figure S5 for Syl1). As shown in Figure 4B, MEG patterns correlated with Syl2 phonetic dissimilarities only after Syl2 onset (reliable effects were observed in three clusters between 100 and 1000 ms post-DP, with the peak effect observed at 448 ms; indicated by horizontal red bars). In contrast the peak correlation with Syl1 phonetic dissimilarities was largely confined to periods in which Syl1 was heard, with a cluster from -200 to +200ms, and peak effects occurring at -136 ms (indicated by horizontal beige bars). This confirms that MEG response patterns represent the phonetic content of the syllables as listeners are hearing them, in line with other, similar demonstrations [26].

We next assessed how neural pattern distances were modulated by syllable predictability by averaging pattern distances over item pairs within each condition and comparing averaged distances between conditions [for a similar approach applied to visual processing, see ref. ,27]. As shown in Figure 4C, following Syl2 onset, prediction strength and congruency interacted to influence MEG pattern distances: stronger predictions resulted in larger MEG pattern distances but only when speech mismatched with predictions (simple effect of Strong - Weak [Mismatch] is shown as shaded grey area in Figure 4C, and the first interaction cluster, 212-292 ms, is plotted as an inset). Thus, as with previous signal magnitude analyses, neural responses after Syl2 onset appear more consistent with prediction error than with sharpened signal computations.

Correlating pattern distances with a graded measure of syllable prediction strength (i.e. p(Syl2|Sy1)) revealed further, convergent evidence for prediction error computations (Figure 4D). Stronger predictions for upcoming speech sounds during Syl2 were associated with opposite effects on MEG pattern distances from 360 to

468 ms, depending on prediction congruency (significant timepoints indicated as horizontal cyan bars). During this time period, correlations between prediction strength and pattern distances were positive when predictions mismatched with heard speech (i.e. neural representations are more informative for speech that mismatched with stronger predictions), and negative when predictions matched heard speech (i.e. less informative representations for speech that matched stronger predictions). These findings are as expected for representations that signal prediction error (Figure 1E right). Individually, correlations within the Matching condition were not significantly different from zero. But within the Mismatching condition, correlations were significantly positive from 320 to 544 ms (shown as shaded grey area in Figure 4D).

We also applied our pattern analysis procedure to MEG sensor-space patterns after the data was transformed into a time-frequency representation of signal power (Figure 4E). Here there was again an interaction between prediction strength and congruency with a peak at 560 ms in the theta band (peak at 4 Hz, extending to higher alpha frequencies). This interaction was driven by smaller MEG pattern distances (i.e. less informative neural representations) for Matching syllables that follow Strong rather than Weak predictions (Figure S2D). Again, this effect is in line with neural responses that signal prediction errors in heard speech. We also applied the same pattern analysis approach to high-frequency gamma activity (52-90 Hz) but did not observe condition-wise differences.

Figure 4

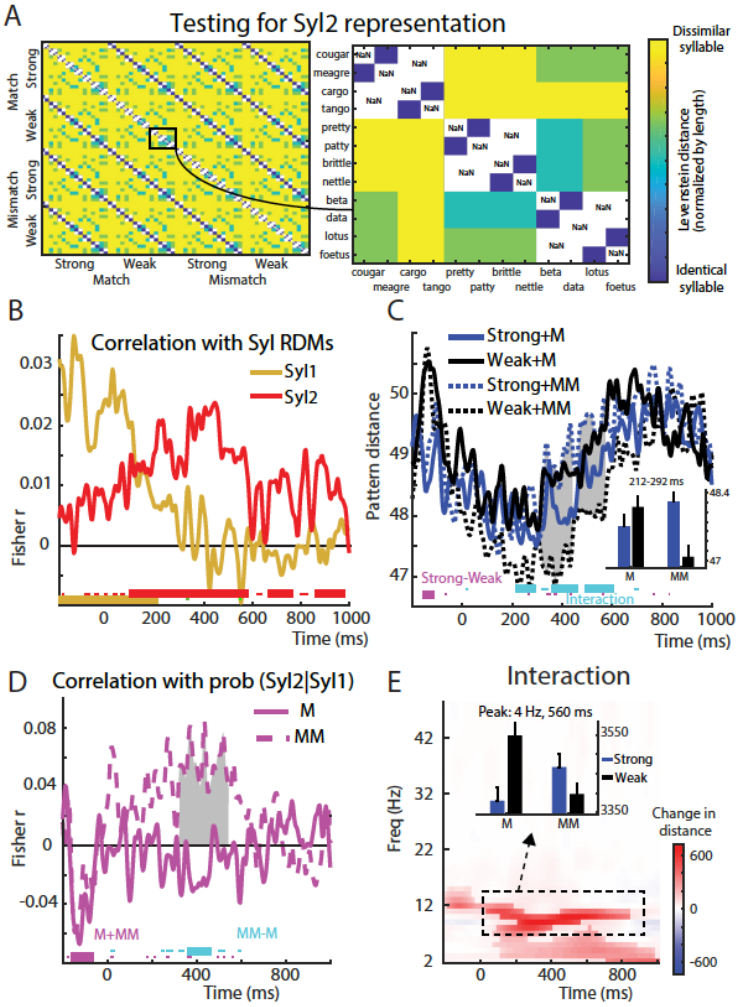

Figure 4 MEG pattern analysis results. (A) Phonetic dissimilarity matrix expressing the normalized Levenshtein distance between phonetic transcriptions of Syl2 for different item pairs. Right panel inset highlights predicted dissimilarity used in representational analyses. (B) Group-averaged correlation between MEG pattern distances and phonetic dissimilarities for Syl2 (in red) and Syl1 (in beige). Horizontal bars indicate timepoints when correlations were significantly different from zero (thick lines show corrected significance at p < .05 clusterwise; thin lines show uncorrected significance at p < .05). (C) Group-averaged MEG pattern distances with larger values indicating more dissimilar MEG response patterns between items. Grey shaded area indicates timepoints when there was a significant difference between Strong and Weak items in the Mismatch condition (p < .05 FWE clusterwise corrected). The inset bar plot shows group means for each condition (and within-subject standard errors as before) after averaging over the temporal extent of the cluster for the interaction contrast. (D) Group-averaged correlations between p(Syl2|Syl1) and MEG pattern distances. Grey shaded area indicates timepoints when there was a significant positive correlation for Mismatch items (p < .05 FWE clusterwise corrected). (E) Group-averaged MEG pattern distances after transforming the MEG signal into time-frequency power. Image depicts the interaction contrast: (Strong-Weak [Mismatch)]) – (Strong-Weak[Match]). Nontransparent colors indicate significance at p < .05 (FWE cluster corrected) while transparent colors indicate p < .05 (uncorrected). Bar graph indicates group means (and within-subject standard errors) after averaging over the temporal and frequency extent of the interaction cluster (black broken outline on the time-frequency image).

fMRI pattern analysis

To localize the neural generators of the MEG pattern analysis effects reported above, we applied a similar pattern analysis approach to spatial searchlights in auditory brain areas in our fMRI data. As with our MEG pattern analysis, we first asked whether fMRI responses contained phonetic information about Syl2 by correlating neural pattern distances with the phonetic dissimilarity between the second syllables of item pairs. As shown in Figure 5A, multivoxel patterns correlated with Syl2 phonetic dissimilarities in HG bilaterally (see Table 1 for MNI space locations).

We next proceeded to examine between-condition differences in neural representations. Rather than directly analysing pattern distances (as with the equivalent MEG analysis above), we opted to analyse a more specific measure of the correlation between neural patterns and Syl2 phonetic dissimilarities. This approach is more optimally suited to measure fMRI responses that are specific to Syl2 as opposed to representing both syllables. This is because while the temporally precise MEG signal can easily resolve neural responses to Syl1 and Syl2, this is not the case for fMRI which integrates sensory information over both syllables. However, by analysing the strength of correlation between fMRI pattern distances and Syl2 phonetic dissimilarities, we can more specifically examine the neural representations of Syl2. Within the left and right HG clusters previously shown in Figure 5A, prediction strength and congruency showed interactive effects on the correlation between multivoxel pattern distances and Syl2 phonetic dissimilarities (shown in Figure 5B; $F(1,20) = 10.00$, $p = .005$). This effect did not reliably differ in magnitude between the two hemispheres (the three-way interaction between prediction strength, congruency and hemisphere was non-significant: $F(1,20) = 0.170$, $p = .684$). Though the interaction effect failed to reach significance in the left hemisphere ($F(1,20) = 3.304$, $p = .084$), the interaction effect was significant in the right hemisphere ($F(1,20) = 7.831$, $p = .011$). While tests of simple effects within each hemisphere were not reliable, the numerical trends are entirely consistent with previous analyses and in line with computational predictions: increasing prediction strength resulted in a numerically weaker correlation for a matching Syl2 ($F(1,20) = 2.85$, $p = .107$) while the opposite numerical difference (i.e. a stronger correlation for

stronger predictions) was observed for mismatching Syl2 items (F(1,20) = 2.70, p = .116).

We also examined whether fMRI responses contained phonetic information about Syl1 by correlating neural pattern distances with the phonetic dissimilarity between the first syllables of item pairs. However, we did not find significant correlations (all clusters p > .6 uncorrected).

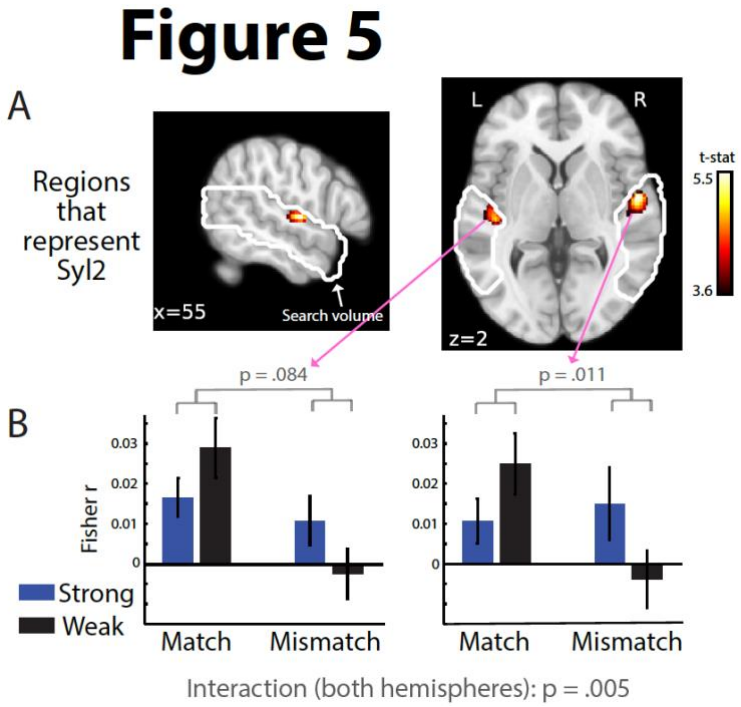

Figure 5 fMRI pattern analysis results. (A) Statistical maps showing voxels in which there was a significant correlation between fMRI pattern distances and phonetic dissimilarities for Syl2 (p < .05 FWE corrected clusterwise). White outline shows search volumes as in Figure 3. (B) Group-averaged correlations (and within-subject standard errors) after averaging over voxels in the left and right hemisphere clusters shown in (A).

MEG responses to non-speech noise replacing strong- and weakly predicted syllables

We also presented stimuli in which Syl2 was replaced with spectrally and intensity (RMS) matched noise. This creates a further opportunity to test the prediction error account. For these stimuli, Syl2 is predicted but absent from the sensory input, which should evoke a negative prediction error for that syllable [28]. According to a prediction error account, neural responses to noise can nonetheless convey information about which stimulus was predicted, particularly when these predictions are strong and specific. Consistent with this, MEG pattern distances after

noise onset were larger when predictions from Syl1 were strong versus weak (Figure 6B). This occurred from 200 to 276 ms after noise onset, in the same frontotemporal sensors as previous MEG analyses (sensor locations shown in Figure 2A), overlapping with time periods when MEG responses contain phonetic information about Syl2 for speech that is physically present (cf. Figure 4B). This is despite the fact that the overall strength of MEG responses after noise onset remained unchanged for 'Strong+Noise' versus 'Weak+Noise' stimuli (magnitude MEG analysis shown in Figure 6A). Note that the strength of MEG responses before Syl2 onset was larger for Strong+Noise versus Weak+Noise items, but as mentioned before, this may simply reflect acoustic (Syl1 duration) differences (see SI Results and Figure S4A).

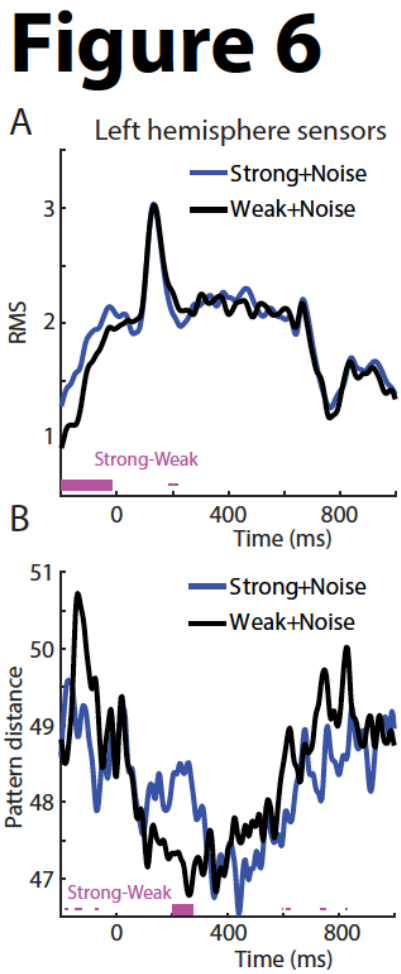

Figure 6 MEG results for Strong+Noise and Weak+Noise stimuli. (A) MEG signal magnitude analysis showing the RMS of the MEG signal across "speech-responsive" sensors in the left hemisphere, timelocked to the onset of the second syllable (Syl2) when predicted syllables are replaced by noise (sensor locations shown in Figure 2A). (B) MEG pattern analysis showing group-averaged pattern distances for second syllables replaced by noise. Thick horizontal bars at the bottom of the graph indicate timepoints when statistical contrasts were significant at a clusterwise threshold of p < .05 FWE corrected (as in Figures 2 and 4).

Discussion

Across multiple imaging modalities (MEG, fMRI), analysis approaches (signal magnitude and pattern), and signal domains (phase-locked, evoked activity and induced, time-frequency MEG responses), we show that neural responses to second syllables in spoken words are modulated by the strength and content of prior knowledge (i.e. predictions for expected speech sounds). We further show that these neural influences of prior knowledge begin around 200 ms after the onset of the second syllable, localise to early auditory regions (in fMRI, bilateral Heschl's gyrus and STG) and are also expressed as changes in low-frequency (theta and alpha) power.

Neural patterns distinguish prediction error from sharpened signal computations

In the current study, the critical analyses used pattern analysis procedures that previous work has shown can unambiguously distinguish between sharpened signal and prediction error accounts [17,20]. By examining the pattern and not just the overall strength of neural signals, responses tuned to the stimulus input features as well as those tuned away from the heard stimulus can be jointly modelled. In this analysis framework, neural response patterns should contain less information about strongly versus weakly predicted speech sounds (see computational simulations in Figure 1E), and this is indeed what we observed for MEG and fMRI responses to familiar words.

While neural representations of second syllables are suppressed for stronger predictions that match heard speech, neural representations of exactly the same syllables show the opposite modulation for second syllables of pseudowords. That is, when predictions mismatch with sensory input, neural representations are enhanced after more strongly- than more weakly-predicting syllables. Our computational simulations confirm that the interaction between prediction strength and match/mismatch is entirely consistent with the operation of prediction error computations [8–11] but cannot be explained by sharpening accounts in which representations of speech can only be enhanced by prior knowledge [5–7]. Our study therefore provides convergent neural evidence – from different imaging

modalities and multiple analysis approaches – that speech perception is supported by the computation of prediction error representations in auditory brain regions.

Prediction error computations during natural listening

Our findings replicate and extend the findings of previous studies that manipulated prior knowledge by presenting matching or nonmatching written words before highly degraded spoken words [17,20,29]. In this previous work, neural representations showed interactive influences of prior knowledge and signal quality, consistent with a prediction error account. We go beyond this previous work by demonstrating prediction error computations in a more natural listening situation. The present experiments are more naturalistic in two respects: Firstly, we presented clear speech rather than the highly degraded (and hence less natural sounding) noise-vocoded words used previously. Secondly, we used an intrinsic manipulation of prior knowledge based on listeners' long-term linguistic knowledge of familiar spoken words rather than an extrinsic manipulation of predictions based on written text. This demonstration of prediction errors during more natural listening situations is important because it directly addresses the concern that previous results reflect a "prediction encouraging" paradigm [21] that would not generalise to other listening situations. Instead, our findings are consistent with the idea that lexical identification operates through prediction error computations and that these are integral to perceptual processing of speech irrespective of the listening situation [3,30–33].

One might argue that our findings fall short of demonstrating prediction error computation in a fully naturalistic listening situation as our stimuli comprised individual spoken words as opposed to connected speech. In other work investigating speech processing during perception of connected speech (e.g. stories), neurophysiological responses (measured by MEG, EEG or electrocorticography) are shown to correlate with various measures of time-varying predictability, including phoneme surprisal [12–15,34], phoneme entropy [14,34] and lexical entropy [12,15,34]. While these findings clearly demonstrate that speech processing is strongly modulated by prior knowledge, consistent with the notion that speech perception is fundamentally a process of Bayesian inference [2], they do not indicate whether the underlying neural computations involve sharpened signals or prediction errors. Consider for example, the common observation of reduced responses to predictable speech sounds. This response reduction is compatible with

either a prediction error account (through the suppression of responses tuned to input features that are predicted) or a sharpened signal mechanism (through the suppression of responses tuned away from the input features; for a more detailed explanation, see Introduction and refs. [5,6,19]).

More recently, studies employing connected speech paradigms have shown that neural representations of speech segments and acoustic features are themselves modulated by predictability [26,35,36]. These studies use an approach analogous to the present pattern analysis since they specifically link neural effects of surprisal and entropy to neural representations of specific segments or acoustic features. However, previous findings appear inconsistent with respect to sharpening and prediction error accounts since some studies show that neural representations are enhanced when predictions are strong [35] while others show the opposite [36] or even effects in both directions at different latencies [26].

These inconsistent results from story listening paradigms therefore suggest that alternative experimental manipulations of listeners' predictions are needed to distinguish between accounts. Our pseudoword condition creates a second situation in which prediction error and sharpened signal computations can be teased apart. Pseudowords are previously unfamiliar to participants, and hence create a unique listening situation in which predictions entirely mismatch with sensory input. Under a sharpened signal account, the strength and pattern of neural representations of speech sounds forming a pseudoword (as compared with a word) should be suppressed, reflecting the low prior probability of hearing these speech sounds. Our sharpened signal simulations indicate this suppression should be more pronounced when speech follows strongly- versus weakly-predicting first syllables. In contrast, under a prediction error account, the exact opposite should occur i.e. enhanced representations for pseudowords, particularly following strongly-predicting first syllables. Neural responses to pseudowords are consistent with this latter pattern and hence are likely to reflect prediction error computations. In our signal magnitude analyses, we observed larger MEG and fMRI responses for pseudowords versus words. For pattern analyses, although we did not observe a reliable main effect of prediction congruency, neural representations of speech for pseudoword items were enhanced following strongly- versus weakly-predicting first syllables. Overall, these pseudoword results again favour a prediction error account.

We have previously argued that larger prediction error responses for pseudowords compared to real words provide a potential signal for novelty detection and pseudoword learning [3,interpreting results from 11,37]. Our demonstration of more informative prediction errors for syllables that mismatch with more strongly-predicting first syllables suggests that such pseudowords might be more readily learned. We note that memory studies using visual stimuli have similarly argued for enhanced learning of face-scene associations that generate larger prediction errors at encoding [38]. Consistent with this proposal, are the present behavioural results from the cued memory recall test conducted after the fMRI scans. This showed that listeners' recall for pseudowords is more accurate for items that strongly mismatched with predictions in the scanner.

Spatiotemporal and spectral profile of prediction error computations

Our results also establish the timing and location of prediction error computations in response to speech. Previous studies using EEG [13], MEG [12–14,26], fMRI [17,39–42] and electrocorticography [15,43] disagree about when and where prediction errors are computed in the cortical hierarchy. Each of these techniques has their strengths but none combines spatiotemporal resolution with wide coverage of the cortex. Perhaps because of this, it remains unclear whether predictive neural computations emerge only once sensory information has been transformed into non-acoustic (e.g. phonetic) representations [12] or whether acoustic representations themselves can support predictive computations [20]. In the present study, we obtained MEG and fMRI responses to the same stimuli, while participants performed the same incidental (pause detection) task to maintain attention. This feature of our study enabled us to map out prediction error computations precisely in both time and space.

In our MEG results, effects of prediction strength and congruency occurred around 200 ms following the onset of the critical second syllable. Note however that our word and pseudoword stimuli are identical until approximately 100 ms after the onset of the second syllable (corresponding to the onset of the subsequent segment). Therefore, relative to when the critical acoustic information became available to listeners, the interaction between prediction strength and congruency occurred with a latency of approximately 100 ms. This latency is compatible with a low-level acoustic locus of prediction error computation but perhaps not early enough

to definitively rule out a higher-level (non-acoustic) locus, if word identification is supported by rapid (< 50 ms) cortical mechanisms [44].

However, our fMRI results enable more definitive conclusions, since searchlight pattern results show prediction effects in primary auditory cortex (Heschl's Gyrus). This localisation to Heschl's Gyrus is striking as it suggests that predictive computations for speech can operate even at the lowest levels of the cortical processing hierarchy, which leaves open the possibility that top-down predictive influences may even extend subcortically [45]. Future work manipulating prediction at different linguistic levels (e.g. sublexical, lexical and supralexical) would be valuable to establish the generality of this finding, and to determine whether these effects are uniquely or differentially localised to specific cortical regions.

In both signal magnitude and pattern analysis of MEG responses, the interaction between prediction strength and congruency occurred in low-frequency neural responses, with a peak in the theta range (3-4 Hz). An influential proposal claims that bottom-up prediction errors are conveyed by high-frequency (gamma) activity while top-down predictions are conveyed by low-frequency (alpha/beta) signals [16,46,47]. This is consistent with the idea that neural representations integrate sensory information over longer timescales at higher cortical levels (where top-down predictions are proposed to originate; see [39,40,48–50]). If the current findings reflect prediction errors as we have argued, then we might have expected modulation in the gamma range, which we did not observe. Instead, our findings are consistent with other work suggesting that prediction errors for speech are conveyed in low-frequency neural signals [14,51]. This does not rule out an additional role for gamma responses. It may be for example that theta and gamma responses are coupled [52,53] and that gamma effects are not observed in the present study due to the generally lower signal-to-noise ratio of MEG responses at higher frequencies [54].

Prediction strength modulates responses to non-speech noises

Finally, we contrasted neural responses to non-speech noises following strongly- and weakly-predicting first syllables. We observed that noise-evoked neural responses conveyed most information about which syllable was predicted when predictions were strong than when weak. This effect emerges 200 ms after speech input in frontotemporal sensors, consistent with a source in Heschl's Gyrus or

neighbouring regions associated with auditory processing. This result is entirely compatible with a prediction error account. If the acoustic features of a syllable are strongly predicted but absent from the input, this will result in negative prediction errors for those features. Thus, in a prediction error account, even an entirely uninformative, non-speech noise can evoke informative neural activity patterns corresponding to predicted speech sounds.

Other evidence consistent with negative prediction errors comes from studies measuring responses to unexpected silence during predictable sequences. For example, omitted speech segments that are strongly predicted based on repetition frequency (in a Mismatch Response design) or sentence context evoke larger brain responses than when predictions are weak [55]. Going beyond effects on neural response magnitude, other work has shown that speech segments in words that are replaced with noise evoke neural representations similar to those evoked by the original speech [56]. This latter demonstration suggests that brain responses to omitted or noise-replaced sensory input do not simply reflect a generic surprise response that functions to signal the presence versus absence of speech sounds [cf. 28]. Rather, they reflect feature specific responses that signal the identity of the speech sounds, as proposed by a prediction error account.

What has been lacking in work to date is direct evidence that speech-like representations evoked by noise are the result of predictive computations. Our study addresses this issue directly as we show that neural representations contain more information about which syllable was predicted when predictions are strong. Thus, in our study we directly link neural restoration of missing speech with the strength of listeners' predictions. As this effect is specific to individual items, it cannot be attributed to a generic surprise response common to all items (which cannot be ruled out in previous studies assessing only response strength). Indeed, our signal magnitude analysis of (item-averaged) MEG responses, which would be expected to detect a generic surprise response to noise, did not show an effect of prediction strength.

It is currently unclear how positive and negative prediction errors might be signalled at the single neuron or neural population level, but it is possible that they are encoded by separate neural populations [28]. In support of this proposal is evidence of neurons in superficial layers of V1 cortex in mice that specifically respond to the absence of visual input [57,58]. In humans, multivoxel fMRI

representations in left inferior frontal regions show negative correlations such that verified predictions and violated predictions for speech segments result in opposite effects on neural pattern similarity [59]. This finding is argued to reflect separate but co-localised neural populations that uniquely represent positive and negative prediction errors. Further evidence from higher-resolution methods (such as laminar fMRI, or intercranial EEG) could be used to establish how positive and negative prediction errors are signalled neurally.

A further question for future research is how prediction errors, both positive and negative, relate to subjective experience. Informal introspection when listening to stimuli in which the second syllable is replaced by noise suggest that predicted but noise-replaced syllables do not result in the subjective experience of speech. One reason why this might be is because perceptual restoration appears to be dependent on there being a degree of acoustic similarity between the absent speech and the replacing noise [60]. Although the noises in our study were spectrally matched to the speech signal, the amplitude profile of the noises was constant over time and differed to the speech temporal envelope. Therefore, perceptual restoration may have been weaker than if we had replaced single segments [as common in previous demonstrations of perceptual restoration; ,56,60,61].

Despite this non-speech subjective experience, we have shown that noise-evoked neural responses contain information on speech content when predictions are strong. This effect occurs in sensors that also respond to intact speech and with a similar latency, consistent with an origin in sensory cortex. Accounts in which perceptual experiences arise primarily from sensory responses [e.g. 62] would need modification to account for this observation – our observation of informative neural representations in sensory regions occurs in a condition in which subjective experiences of speech are absent. Because prediction errors function to update predictions in higher levels of the hierarchy [3,8], it could be that perceptual outcomes arise from the combination of informative prediction errors in sensory cortex with higher-level lexical or semantic representations in non-sensory regions. This is consistent with the view that subjective experience emerges not in sensory regions alone but also in higher-level cortex [63,64]. Future work relating neural responses to subjective reports of the presence or absence of speech information, and to ratings of perceived clarity in single trials [65] would be valuable to address this issue.

Methods

Participants

40 participants (19 in the MEG experiment, 21 in the fMRI experiment) were tested after being informed of the study's procedure, which was approved by the Cambridge Psychology Research Ethics Committee. All were right-handed, native speakers of English, aged between 18 and 40 years and had no self-reported history of hearing impairment or neurological disease. The mean age in the MEG experiment was 25 years (SD = 4.63; 12 female, 7 male) and 23 years in the fMRI experiment (SD = 3.14; 13 female, 8 male).

Stimuli

Spoken stimuli were 16-bit, 44.1 kHz recordings of a male speaker of southern British English and their duration ranged from 388 to 967 ms (mean = 621, SD = 107). A set of 64 bisyllabic words (Match items) were first selected from the CELEX database [66] based on the probability of the second syllable (Syl2) conditioned on the first syllable (Syl1):

$$p(Syl2|Syl1) = \frac{\sum freq(words\ matching\ both\ syllables)}{\sum freq(words\ matching\ first\ syllable)} \qquad Eq.\ 1$$

For this we used syllabified phonetic transcriptions in CELEX such that the first syllable t{N, for example, in words such as *tango* and *tangle* were considered to match the speech signal since all these words share the same first syllable t{N. However, words such as "tank" were not considered as matching since this word consists of the single syllable t{Nk. Words were selected as sets of eight items (one example item set is shown in Figure 1A). Within a set of eight items, each word had a unique Syl1 that strongly or weakly predicted one of two Syl2 syllables. By cross-splicing the first and second syllables of these words, we were able to create a set of pseudowords (Mismatch items) that contained the same Syl2 syllables as the real words.

To ensure that Syl2 syllables shared between items were acoustically identical, all four recorded syllables were combined using audio morphing using STRAIGHT software [67] implemented in Matlab (The Mathworks Inc). This software

decomposes speech signals into source information and spectral information, and permits high quality speech resynthesis based on modified versions of these representations. This enables flexible averaging and interpolation of parameter values that can generate acoustically intermediate speech tokens [37,for application see 68]. Exploiting this capability of STRAIGHT, all words and pseudowords sharing the same Syl2 were constructed to be acoustically identical following Syl1 (by averaging STRAIGHT parameters across the four instances of the same Syl2 syllable within a set and splicing the resulting syllable onto Syl1). To ensure that all syllables sounded natural in these contexts, we constrained word selection such that all Syl2 syllables within a set started with the same speech segment. In this way, we could cross-splice syllables without conflicting co-articulatory information at the onset of Syl2. As a result, the point at which words and pseudowords diverged (the divergence point) occurred not at the onset of Syl2 but one speech segment later (post divergence point speech segments highlighted as bold in Figure 1A). Additional stimuli were derived by replacing the Syl1, Syl2, or both syllables, with spectrally and intensity (RMS) matched noise. In total there were eight sets of items and therefore 240 stimuli (32 items in each of the following conditions: Strong+Match, Weak+Match, Strong+Mismatch, Weak+Mismatch; 32 each of Strong+Noise, Weak+Noise; 32 of Noise+Syl2; 16 of Noise+Noise). For analysis of stimulus properties, see supplementary Results.

Before the experiment, participants completed a brief practice session lasting approximately three minutes that contained examples of all the stimulus types included (spoken words, pseudowords with and without noise) but using different items to the main experiment. Stimulus delivery was controlled with Psychtoolbox [69] scripts in Matlab.

Procedure

Stimulus presentation and task procedure was nearly identical for MEG and fMRI listeners. On each trial, listeners heard one of the spoken items separated by a stimulus onset asynchrony (SOA) of 2.5 sec (see Figure S1A). For the MEG experiment, this SOA was jittered by adding a random time interval of ±100 ms. For the fMRI experiment, a constant SOA was used, and stimuli were presented at the offset of the scans (sparse imaging sequence). Participants were asked to look at a

fixation cross in the centre of the screen and respond as quickly and accurately as possible whenever they heard a brief pause in the speech stimuli. Pauses consisted of an additional 200 ms silence inserted between Syl1 and Syl2. Pilot testing revealed that pause detection was more difficult when one or both syllables were replaced by noise. To better equate performance, the duration of the pause was lengthened to 300 ms (for the Noise+Noise condition) and 400 ms (for the Strong+Noise, Weak+Noise and Noise+Syl2 conditions).

Trials were randomly ordered during each of five presentation blocks of 288 trials. Each block consisted of a single presentation of all stimuli plus 'Pause' stimuli. Across all five blocks, the order of 'Pause' and 'No Pause' items was completely randomised; in total there was one 'Pause' item for every six 'No Pause' items, with this ratio constant across stimulus type (Strong+Match, Weak+Match etc.). Participants received feedback on performance (% correct) at the end of each block.

Computational simulations

Both sharpened signal and prediction error computations have the goal of implementing Bayes perceptual inference for spoken words [2,9]:

$$p(Word_i|Evidence) = \frac{p(Word_i) \times p(Evidence|Word_i)}{\sum_{j=1}^{j=n} p(Word_j) \times p(Evidence|Word_j)} \qquad Eq.\ 2$$

This equation computes the conditional (posterior) probability of each word, given their prior probabilities (frequency of occurrence) and the available sensory evidence. We modelled uncertainty in the sensory evidence based on the acoustic similarity between individual speech segments. Acoustic representations were obtained from a large set of 1024 words spoken by the same speaker as for the present stimuli. These stimuli comprised recordings from previous studies [65,70,71] as well as the 32 Strong Match items and 32 Weak Match items from the current study. From these stimuli, we computed acoustic energy for individual speech segments (phonemes): 48 unique segments in total, averaged over 3297 repeated tokens (median token count = 54). Acoustic energy was expressed as a function of time, frequency and spectrotemporal modulations [72], as computed by the nsltools toolbox in Matlab [http://nsl.isr.umd.edu/downloads.html; for details see 20].

Segment onset times were obtained using a forced-alignment algorithm included as part of BAS software [73; https://clarin.phonetik.uni-muenchen.de/BASWebServices/interface/WebMAUSGeneral]. Acoustic representations were vectorized and averaged over multiple productions of the same segment. We then obtained a between-segment similarity matrix using negative Euclidean distances and normalized each row of this matrix using the softmax function (combined with a temperature parameter *T*) such that each row could be interpreted as segment likelihood probabilities:

$$p(Segment_i) = \frac{\exp\,(-dT)}{\sum_{i=1}^{i=n} \exp\,(-dT)} \qquad Eq.\ 3$$

where *d* denotes the Euclidean distance. From these segment likelihoods, we could compute the sensory evidence for a word by applying the product rule over word segments [see 2]. The sensory evidence for an unfolding word will be strong if its constituent segments match internal representations that are acoustically dissimilar to other speech sounds in the language. It will also be strong if there are few word competitors sharing the same speech segments. Given that our stimulus set consisted of clear speech recordings, a reasonable assumption is that individual segment likelihoods are close to one (indicating high certainty). Nonetheless, even clear speech segments will be perceived with momentary ambiguities as sub-phonemic information unfolds over the duration of a segment. In the absence of human sub-phonemic confusion data [74] for the British accent of the present stimuli, we scaled acoustic similarities to simulate a range of overall sensory uncertainty levels by varying the Softmax temperature parameter. The same qualitative patterns were present over a range of sensory uncertainty levels (Figure S3). The one exception to this is apparent for simulations with the highest degree of sensory uncertainty for which prediction error representations in the Match condition are enhanced relative to simulations with reduced sensory uncertainty (compare the height of the first bar in each of the bottom row of plots in Figure S3B). The effect of this is that – under high uncertainty – results show a reverse pattern with enhanced neural representations for Strong versus Weak items. This is consistent with previous modelling and experimental data [17,20] and is explained by an increase in the informativeness of prediction errors that occurs when strong predictions match noisy or ambiguous sensory input: Even though speech segments are accurately predicted, their *acoustic form* is not as expected (deviating from clear speech).

Note that our stimuli were selected based on syllable conditional probabilities p(Syl2|Syl1), which used the syllabified phonetic transcriptions in CELEX. For consistency, we therefore incorporated the syllable boundaries from CELEX into our model simulations. We achieved this by adding a separate segment to the model's inventory of segments, representing the boundary between syllables. Thus, an item like "bingo" was represented by six segments in total (five speech sounds plus the boundary between the two component syllables). In Figure 1B and 1C, we omit the syllable boundary segment for display purposes.

To simulate speech processing as each speech segment in our stimuli was heard, we used Bayes theorem to compute the posterior probability distribution over all words in the lexicon. Then to compute predictions for each upcoming speech segment, we summed posterior probabilities over words sharing the same segment. These segment predictions were then multiplied by individual segment likelihoods (derived from acoustic similarity as explained above), to simulate the sharpened signal computation (normalizing to sum to one). For simulating the prediction error computation, segment predictions were instead subtracted from segment likelihoods. For analysis of the simulated representations, pattern distances were computed as the Euclidean distance between model signals for pairs of items at the deviation point. For the signal magnitude analysis, we analysed model representations specifically for the speech segment that was heard at the divergence point.

MEG acquisition and analysis

Magnetic fields were recorded with a VectorView system (Elekta Neuromag, Helsinki, Finland) containing two orthogonal planar gradiometers at each of 102 positions within a hemispheric array. Data were also acquired by magnetometer and EEG sensors. However, only data from the planar gradiometers were analysed as these sensors have maximum sensitivity to cortical sources directly under them and are therefore less sensitive to noise artifacts [75]. To monitor eye and heart activity, EOG and ECG signals were recorded with bipolar electrodes.

MEG data were processed using the temporal extension of Signal Source Separation [76] in Maxfilter software to suppress noise sources, compensate for motion, and reconstruct any bad sensors. Also using MaxFilter, the data were transformed to a common coordinate frame for each participant separately (to compensate for changes in head position between blocks). Subsequent processing

was done in SPM12 (Wellcome Trust Centre for Neuroimaging, London, UK), FieldTrip (Donders Institute for Brain, Cognition and Behaviour, Radboud University Nijmegen, the Netherlands) and The Decoding Toolbox [77] implemented in Matlab.

MEG data were downsampled to 250 Hz and ICA used to remove eye and heart artefacts (based on an automatic procedure correlating the component time-series with EOG and ECG signals). When epoching, we retained only “no pause” trials. MEG recordings were epoched from -1700 ms to 2000 ms relative to the onset of Syl2 and epochs with large amplitude signals were discarded (time- and channel-averaged power larger than 2 standard deviations from the condition-specific mean for signal magnitude analysis; power larger than 3 standard deviations from the pooled mean for pattern analysis). For signal magnitude (evoked response) analyses only, the data were baseline-corrected from -750 to -500 ms relative to Syl2 onset; this corresponds to the silence period before speech onset (since the duration of Syl1 ranged from 130 to 479 ms; see Figure S4C for distribution of Syl1 duration).

For time-frequency analysis, we computed the power between 2 and 48 Hz (in 1 Hz steps) by convolving the data from each trial with Morlet wavelets of 7 cycles. To analyse high frequency activity (52-90 Hz), we used multi-taper estimation (±10 Hz smoothing, 200 ms time-windows with a step size of 20 ms). We analysed differences in power attributable to our experimental manipulations without baseline normalization. For time-domain analyses, the data were additionally low-pass filtered below 30 Hz prior to trial averaging. Note that in the case of signal magnitude analyses, MEG responses reflect the average of 160 trials (or 80 in the case of Noise+Noise items) before outlier removal (5 repetitions × 32 items per stimulus type) while for pattern analyses, MEG responses reflect the average of 5 repetitions (since here we analyze item-specific responses). Subsequent analysis was based on the period immediately before and after Syl2 onset (-200 to 1000 ms).

For signal magnitude (evoked response) analysis, the MEG data across the sensor array were summarized as the root mean square (RMS) over the 20 sensors with the largest evoked response (separately in each participant and hemisphere). The same sensors were used when analysing time-frequency power. For pattern analyses, neural pattern distances were computed by taking the Euclidean distance between sensor patterns (over the entire 204 sensor-array) evoked by each pair of items in the relevant stimulus set. To assess whether MEG responses reflected the

phonetic information about the syllables, neural pattern distances were correlated with the phonetic dissimilarities between the syllables of item pairs using Fisher-transformed Spearman's correlations. To compute the phonetic dissimilarities we used the Levenshtein distance between the phonetic transcriptions for each syllable, normalized by the maximum number of segments within the two syllables being compared; shown in Figure 4A for Syl2 and Figure S5 for Syl1 [see 71 for a similar method applied to scoring phonetic responses]. To maximize statistical power for this particular analysis, correlations were computed both across- and within-condition (see Figure 4A). As shown in Figure 4A, we also excluded dissimilarity of item pairs such as "cargar" and "cougo" since similar but opposite prediction errors are evoked during Syl2 of these items. For example, for "cargar", listeners predict "-go" but hear "-gar". For "cougo", listeners predict "-gar" but hear "-go". The pattern of prediction error in these two cases is identical, albeit opposite in polarity. Given uncertainty on how the polarity of prediction errors is encoded in neural responses [28], we exclude these pseudoword item pairs from pattern analysis of our neural data and model simulations. We also exclude the corresponding word item pairs (e.g. "cougar" and "cargo"; shown as NaNs in Figure 4A).

When correlating syllable conditional probabilities with MEG responses (either magnitude-based or pattern-based measures), we also used Fisher-transformed Spearman's correlations. For pattern analysis, in which the dependent measures reflect pattern distances for pairs of items, we averaged syllable conditional probabilities for the items in each pair of words (after log transformation).

For both signal magnitude (RMS signals, time-frequency power or Spearman correlations) and pattern analyses (pattern distances or Spearman correlations), group-level one-sample t-tests were performed for each timepoint (and frequency bin when relevant) while controlling the family-wise error (FWE) rate using a non-parametric cluster-based permutation procedure based on 5000 iterations [78]. These tests were performed on contrasts of the data, testing for the main effects and interactions in our experimental design, as well as any simple effects. Reported effects were obtained by using a cluster defining height threshold of $p < .05$ with a cluster t-sum threshold of $p < .05$ (FWE corrected), unless otherwise stated.

fMRI acquisition and analysis

Imaging data were collected on a Siemens 3 Tesla Prisma MRI scanner (http://www.siemens.com). A total of 291 echo planar imaging (EPI) volumes were acquired in each of 5 scanning runs, using a 32-channel head coil and a multiband sparse imaging sequence (TR = 2.50 sec; TA = 1.135 sec; TE = 30 ms; 48 slices covering the whole brain; flip angle = 78 deg; in-plane resolution = 3 × 3 mm; matrix size = 64 × 64; echo spacing = 0.5 ms; inter-slice gap = 25%). After the third run, field maps were acquired (short TE = 10 ms; long TE = 12.46 ms). The experimental session commenced with the acquisition of a high-resolution T1-weighted structural MRI scan (TR = 2250 ms; TE = 2.99 ms; flip angle = 9°; 1 mm isotropic resolution; matrix size: 256 × 240 × 192 mm; GRAPPA acceleration factor PE = 2; Reference lines PE = 24).

fMRI pre-processing was performed in SPM12. After discarding the first four volumes to allow for magnetic saturation effects, the remaining images were realigned and unwarped to the first volume to correct for movement of participants during scanning. Also at the unwarping stage, the acquired field maps were used to correct for geometric distortions in the EPI due to magnetic field variations. Realigned images were co-registered to the mean functional image and then subjected to statistical analysis. For signal magnitude analysis, prior to further processing, images were also normalized to the Montreal Neurological Institute (MNI) template image using the parameters from the segmentation of the structural image (resampled resolution: 2 × 2 × 2 mm) and smoothed with a Gaussian kernel of 6 mm full-width at half-maximum. For pattern analysis, normalization and smoothing were performed only after computing pattern distances.

Statistical analysis was based on the general linear model (GLM) of each participant's fMRI time series, using a 1/128 second highpass filter and AR1 correction for auto-correlation. The design matrix comprised the auditory stimulus events (onset of the spoken words), each modeled as a stick (delta) function and convolved with the canonical haemodynamic response function specified in SPM software. For signal magnitude analysis, separate columns were specified for each of the stimulus types in addition to a column for button presses (replicated for each

of the five experimental blocks). For pattern analysis, the design matrix was identical but separate columns were specified for each individual item (except for Noise+Noise items which was specified as a single column since these stimuli had largely imperceptible differences based only on the spectrum and RMS levels of the word items that they were matched to).

Pattern analysis was performed using searchlight analysis [79] as implemented in the Decoding toolbox, using spheres with a radius of 8 mm and constrained to voxels within the whole-brain mask generated by SPM during model estimation. Pattern distances were computed using the cross-validated Mahalanobis distance [80]. This 'Crossnobis' distance is equivalent to the (cross-validated) Euclidean distance, normalized by the noise covariance between voxels (estimated from the GLM residuals). Cross-validation ensures that the expected pattern distance is zero if two voxel patterns are not statistically different from each other, making it a readily interpretable distance measure. Note that because of this cross-validation, the Crossnobis distance can sometimes be negative if it's true value is close to zero in the presence of noise. The Crossnobis distance has been demonstrated to be a more reliable and accurate metric for characterizing multivoxel patterns than the correlation or Euclidean distance [80]. To assess whether fMRI responses reflected the phonetic information about Syl2, neural pattern distances were Spearman correlated with the phonetic dissimilarities between Syl2 portions of item pairs using the same Levenshtein distance measure as the MEG analysis (shown in Figure 4A).

For both signal magnitude (contrast images from first-level models or Spearman correlations) and pattern analyses (Spearman correlations), group-level one-sample t-tests were performed for each voxel within a mask covering superior and middle temporal regions (shown in Figure 3A). Inference was conducted parametrically, controlling the family-wise error (FWE) rate using random field theory. Reported effects were obtained by using a cluster defining height threshold of $p < .001$ with a cluster extent threshold of $p < .05$ (FWE corrected), unless otherwise stated.

Data availability statement

Stimuli, data and analysis scripts will be made available on OSF upon publication of this manuscript.

References

1. Norris D, McQueen JM, Cutler A. Prediction, Bayesian inference and feedback in speech recognition. Language, Cognition and Neuroscience. 2015;3798: 1–15. doi:10.1080/23273798.2015.1081703

2. Norris D, McQueen JM. Shortlist B: a Bayesian model of continuous speech recognition. Psychological review. 2008;115: 357–95. doi:10.1037/0033-295X.115.2.357

3. Davis MH, Sohoglu E. Three functions of prediction error for Bayesian inference in speech perception. Cog Neuro. MIT Press; 2020. pp. 177–192.

4. McClelland JL, Elman JL. The TRACE model of speech perception. Cognitive Psychology. 1986;18: 1–86. doi:10.1016/0010-0285(86)90015-0

5. Lange FP de, Heilbron M, Kok P. How Do Expectations Shape Perception? Trends in Cognitive Sciences. 2018;22: 764–779. doi:10.1016/j.tics.2018.06.002

6. Murray SO, Schrater P, Kersten D. Perceptual grouping and the interactions between visual cortical areas. Neural networks : the official journal of the International Neural Network Society. 2004;17: 695–705. doi:10.1016/j.neunet.2004.03.010

7. Aitken F, Turner G, Kok P. Prior Expectations of Motion Direction Modulate Early Sensory Processing. The Journal of Neuroscience. 2020;40: 6389–6397. doi:10.1523/JNEUROSCI.0537-20.2020

8. Rao RP, Ballard DH. Predictive coding in the visual cortex: a functional interpretation of some extra-classical receptive-field effects. Nature neuroscience. 1999;2: 79–87. doi:10.1038/4580

9. Aitchison L, Lengyel M. With or without you: predictive coding and Bayesian inference in the brain. Current Opinion in Neurobiology. 2017;46: 219–227. doi:10.1016/j.conb.2017.08.010

10. Friston K. A theory of cortical responses. Philosophical transactions of the Royal Society of London Series B, Biological sciences. 2005;360: 815–36. doi:10.1098/rstb.2005.1622

11. Gagnepain P, Henson RN, Davis MH. Temporal Predictive Codes for Spoken Words in Auditory Cortex. Current biology : CB. 2012;22: 1–7. doi:10.1016/j.cub.2012.02.015

12. Brodbeck C, Hong LE, Simon JZ. Rapid Transformation from Auditory to Linguistic Representations of Continuous Speech. Current biology : CB. 2018;28: 3976-3983.e5. doi:10.1016/j.cub.2018.10.042

13. Heilbron M, Armeni K, Schoffelen J-M, Hagoort P, de Lange FP. A hierarchy of linguistic predictions during natural language comprehension. Proc Natl Acad Sci USA. 2022;119: e2201968119. doi:10.1073/pnas.2201968119

14. Donhauser PW, Baillet S. Two Distinct Neural Timescales. Neuron. 2020; 1–9. doi:10.1016/j.neuron.2019.10.019

15. Keshishian M, Akkol S, Herrero J, Bickel S, Mehta AD, Mesgarani N. Joint, distributed and hierarchically organized encoding of linguistic features in the human auditory cortex. Nat Hum Behav. 2023; 1–14. doi:10.1038/s41562-023-01520-0

16. Bastos AMM, Usrey WMM, Adams RAA, Mangun GRR, Fries P, Friston KJJ. Canonical Microcircuits for Predictive Coding. Neuron. 2012;76: 695–711. doi:10.1016/j.neuron.2012.10.038

17. Blank H, Davis MH. Prediction Errors but Not Sharpened Signals Simulate Multivoxel fMRI Patterns during Speech Perception. PLoS biology. 2016;14: e1002577. doi:10.1371/journal.pbio.1002577

18. de Lange FP, Schmitt L-M, Heilbron M. Reconstructing the predictive architecture of the mind and brain. Trends in Cognitive Sciences. 2022;26: 1018–1019. doi:10.1016/j.tics.2022.08.007

19. Luthra S, Li MYC, You H, Brodbeck C, Magnuson JS. Does signal reduction imply predictive coding in models of spoken word recognition? Psychonomic bulletin & review. 2021. doi:10.3758/s13423-021-01924-x

20. Sohoglu E, Davis MH. Rapid computations of spectrotemporal prediction error support perception of degraded speech. eLife. 2020;9: 1–25. doi:10.7554/eLife.58077

21. Huettig F, Mani N. Is prediction necessary to understand language? Probably not. Language, Cognition and Neuroscience. 2016;31: 19–31. doi:10.1080/23273798.2015.1072223

22. Gwilliams L, Davis M. Extracting language content from speech sounds: An information theoretic approach. Springer Handbook of Auditory Research. Springer; 2022. pp. 113–139.

23. Grosjean F. Spoken word recognition processes and the gating paradigm. Perception & Psychophysics. 1980;28: 267–283. doi:10.3758/BF03204386

24. Luce PA, Pisoni DB. Recognizing spoken words: the neighborhood activation model. Ear and hearing. 1998;19: 1–36. doi:10.1097/00003446-199802000-00001

25. Loftus GR, Masson MEJ. Using confidence intervals in within-subject designs. Psychonomic Bulletin & Review. 1994;1: 476–490. doi:10.3758/BF03210951

26. Gwilliams L, King J-R, Marantz A, Poeppel D. Neural dynamics of phoneme sequences reveal position-invariant code for content and order. Nat Commun. 2022;13: 6606. doi:10.1038/s41467-022-34326-1

27. Hebart MN, Bankson BB, Harel A, Baker CI, Cichy RM. The representational dynamics of task and object processing in humans. eLife. 2018;7: 1–21. doi:10.7554/eLife.32816

28. Keller GB, Mrsic-Flogel TD. Predictive Processing: A Canonical Cortical Computation. Neuron. 2018;100: 424–435. doi:10.1016/j.neuron.2018.10.003

29. Blank H, Spangenberg M, Davis MH. Neural Prediction Errors Distinguish Perception and Misperception of Speech. The Journal of neuroscience : the official journal of the Society for Neuroscience. 2018;38: 6076–6089. doi:10.1523/jneurosci.3258-17.2018

30. Clark A. Whatever next? Predictive brains, situated agents, and the future of cognitive science. Behavioral and Brain Sciences. 2013;36: 1–24. doi:10.1017/S0140525X12000477

31. Barascud N, Pearce MT, Griffiths TD, Friston KJ, Chait M. Brain responses in humans reveal ideal observer-like sensitivity to complex acoustic patterns. Proceedings of the National Academy of Sciences of the United States of America. 2016;113: E616-25. doi:10.1073/pnas.1508523113

32. Friston K. Does predictive coding have a future? Nature Neuroscience. 2018;21: 1019–1021. doi:10.1038/s41593-018-0200-7

33. Kuperberg GR, Jaeger TF. What do we mean by prediction in language comprehension? Language Cognition & Neuroscience. 2016;31: 32–59. doi:10.1080/23273798.2015.1102299

34. Brodbeck C, Bhattasali S, Cruz Heredia AA, Resnik P, Simon JZ, Lau E. Parallel processing in speech perception with local and global representations of linguistic context. eLife. 2022;11: e72056. doi:10.7554/eLife.72056

35. Broderick MP, Anderson AJ, Lalor EC. Semantic Context Enhances the Early Auditory Encoding of Natural Speech. The Journal of Neuroscience. 2019;39: 7564–7575. doi:10.1523/JNEUROSCI.0584-19.2019

36. Tezcan F, Weissbart H, Martin AE. A tradeoff between acoustic and linguistic feature encoding in spoken language comprehension. Peelle JE, King AJ, editors. eLife. 2023;12: e82386. doi:10.7554/eLife.82386

37. Wang YC, Sohoglu E, Gilbert RA, Henson RN, Davis MH. Predictive Neural Computations Support Spoken Word Recognition: Evidence from MEG and Competitor Priming. The Journal of neuroscience : the official journal of the Society for Neuroscience. 2021;41: 6919–6932. doi:10.1523/JNEUROSCI.1685-20.2021

38. Greve A, Cooper E, Kaula A, Anderson MC, Henson R. Does prediction error drive one-shot declarative learning? Journal of Memory and Language. 2017;94: 149–165. doi:10.1016/j.jml.2016.11.001

39. Schmitt L-M, Erb J, Tune S, Rysop AU, Hartwigsen G, Obleser J. Predicting speech from a cortical hierarchy of event-based time scales. Science Advances. 2021;7: 2020.12.19.423616. doi:10.1126/sciadv.abi6070

40. Caucheteux C, Gramfort A, King J-R. Evidence of a predictive coding hierarchy in the human brain listening to speech. Nat Hum Behav. 2023; 1–12. doi:10.1038/s41562-022-01516-2

41. Schrimpf M, Blank IA, Tuckute G, Kauf C, Hosseini EA, Kanwisher N, et al. The neural architecture of language: Integrative modeling converges on predictive

processing. Proc Natl Acad Sci USA. 2021;118: e2105646118. doi:10.1073/pnas.2105646118

42. Frank SL, Willems RM. Word predictability and semantic similarity show distinct patterns of brain activity during language comprehension. Language, Cognition and Neuroscience. 2017;32: 1192–1203. doi:10.1080/23273798.2017.1323109

43. Goldstein A, Zada Z, Buchnik E, Schain M, Price A, Aubrey B, et al. Shared computational principles for language processing in humans and deep language models. Nat Neurosci. 2022;25: 369–380. doi:10.1038/s41593-022-01026-4

44. MacGregor LJ, Pulvermüller F, van Casteren M, Shtyrov Y. Ultra-rapid access to words in the brain. Nature communications. 2012;3: 711. doi:10.1038/ncomms1715

45. Tabas A, Mihai G, Kiebel S, Trampel R, von Kriegstein K. Abstract rules drive adaptation in the subcortical sensory pathway. Shinn-Cunningham BG, Griffiths TD, Malmierca MS, editors. eLife. 2020;9: e64501. doi:10.7554/eLife.64501

46. Arnal LH, Wyart V, Giraud A-L. Transitions in neural oscillations reflect prediction errors generated in audiovisual speech. Nature neuroscience. 2011;14: 797–801. doi:10.1038/nn.2810

47. Sedley W, Gander PE, Kumar S, Kovach CK, Oya H, Kawasaki H, et al. Neural signatures of perceptual inference. eLife. 2016;5: 1–13. doi:10.7554/eLife.11476

48. Lerner Y, Honey CJ, Silbert LJ, Hasson U. Topographic mapping of a hierarchy of temporal receptive windows using a narrated story. The Journal of neuroscience : the official journal of the Society for Neuroscience. 2011;31: 2906–15. doi:10.1523/JNEUROSCI.3684-10.2011

49. Honey CJ, Thesen T, Donner TH, Silbert LJ, Carlson CE, Devinsky O, et al. Slow cortical dynamics and the accumulation of information over long timescales. Neuron. 2012;76: 423–34. doi:10.1016/j.neuron.2012.08.011

50. Norman-Haignere SV, Long LK, Devinsky O, Doyle W, Irobunda I, Merricks EM, et al. Multiscale temporal integration organizes hierarchical computation in human auditory cortex. Nature Human Behaviour. 2022. doi:10.1038/s41562-021-01261-y

51. Di Liberto GM, Crosse MJ, Lalor EC. Cortical Measures of Phoneme-Level Speech Encoding Correlate with the Perceived Clarity of Natural Speech. eNeuro. 2018;5: ENEURO.0084-18.2018. doi:10.1523/ENEURO.0084-18.2018

52. Giraud A-L, Poeppel D. Cortical oscillations and speech processing: emerging computational principles and operations. Nature Neuroscience. 2012 [cited 19 Mar 2012]. doi:10.1038/nn.3063

53. Canolty RT, Edwards E, Dalal SS, Soltani M, Nagarajan SS, Berger MS, et al. High gamma power is phase-locked to theta oscillations in human neocortex. Science (New York, NY). 2006;313: 1626–8. doi:10.1126/science.1128115

54. Sedley W, Teki S, Kumar S, Overath T, Barnes GR, Griffiths TD. Gamma band pitch responses in human auditory cortex measured with magnetoencephalography. Neuroimage. 2012;59: 1904–1911. doi:10.1016/j.neuroimage.2011.08.098

55. Bendixen A, Scharinger M, Strauß A, Obleser J. Prediction in the service of comprehension: Modulated early brain responses to omitted speech segments. Cortex. 2014;53: 9–26. doi:10.1016/j.cortex.2014.01.001

56. Leonard MK, Baud MO, Sjerps MJ, Chang EF. Perceptual restoration of masked speech in human cortex. Nature Communications. 2016;7: 13619. doi:10.1038/ncomms13619

57. Keller GB, Bonhoeffer T, Hübener M. Sensorimotor Mismatch Signals in Primary Visual Cortex of the Behaving Mouse. Neuron. 2012;74: 809–815. doi:10.1016/j.neuron.2012.03.040

58. Fiser A, Mahringer D, Oyibo HK, Petersen AV, Leinweber M, Keller GB. Experience-dependent spatial expectations in mouse visual cortex. Nat Neurosci. 2016;19: 1658–1664. doi:10.1038/nn.4385

59. Cope TE, Sohoglu E, Peterson KA, Jones PS, Rua C, Passamonti L, et al. Temporal lobe perceptual predictions for speech are instantiated in motor cortex and reconciled by inferior frontal cortex. Cell Reports. 2023;42: 112422. doi:10.1016/j.celrep.2023.112422

60. Samuel AG. Phonemic restoration: insights from a new methodology. Journal of experimental psychology General. 1981;110: 474–94.

61. Warren R. Perceptual restoration of missing speech sounds. Science. 1970;167: 392–393.

62. Hatamimajoumerd E, Ratan Murty NA, Pitts M, Cohen MA. Decoding perceptual awareness across the brain with a no-report fMRI masking paradigm. Current Biology. 2022;32: 4139-4149.e4. doi:10.1016/j.cub.2022.07.068

63. Mashour GA, Roelfsema P, Changeux J-P, Dehaene S. Conscious Processing and the Global Neuronal Workspace Hypothesis. Neuron. 2020;105: 776–798. doi:10.1016/j.neuron.2020.01.026

64. Banellis L, Sokoliuk R, Wild CJ, Bowman H, Cruse D. Event-related potentials reflect prediction errors and pop-out during comprehension of degraded speech. Neuroscience of Consciousness. 2020;2020: 1–13. doi:10.1093/nc/niaa022

65. Sohoglu E, Peelle JE, Carlyon RP, Davis MH. Predictive Top-Down Integration of Prior Knowledge during Speech Perception. The Journal of neuroscience : the official journal of the Society for Neuroscience. 2012;32: 8443–8453. doi:10.1523/JNEUROSCI.5069-11.2012

66. Baayen RH, Piepenbrock R, Van Rijn H. The CELEX lexical database (CD-ROM). Philadelphia Linguistics Data Consortium University of Pennsylvania. 1993.

67. Kawahara H. STRAIGHT, exploitation of the other aspect of VOCODER: Perceptually isomorphic decomposition of speech sounds. Acoust Sci & Tech. 2006;27: 349–353. doi:10.1250/ast.27.349

68. Rogers JC, Davis MH. Inferior Frontal Cortex Contributions to the Recognition of Spoken Words and Their Constituent Speech Sounds. Journal of cognitive neuroscience. 2017;25: 1–18. doi:10.1162/jocn_a_01096

69. Brainard DH. The Psychophysics Toolbox. Spatial Vision. 1997;10: 433–436. doi:10.1163/156856897X00357

70. Sohoglu E, Peelle JE, Carlyon RP, Davis MH. Top-down influences of written text on perceived clarity of degraded speech. Journal of Experimental Psychology: Human Perception and Performance. 2014;40: 186–199. doi:10.1037/a0033206

71. Sohoglu E, Davis MH. Perceptual learning of degraded speech by minimizing prediction error. Proceedings of the National Academy of Sciences. 2016;113: E1747–E1756. doi:10.1073/pnas.1523266113

72. Chi T, Ru P, Shamma SA. Multiresolution spectrotemporal analysis of complex sounds. The Journal of the Acoustical Society of America. 2005;118: 887–906. doi:10.1121/1.1945807

73. Kisler T, Reichel U, Schiel F. Multilingual processing of speech via web services. Computer Speech & Language. 2017;45: 326–347. doi:10.1016/j.csl.2017.01.005

74. Warner N, McQueen JM, Cutler A. Tracking perception of the sounds of English. The Journal of the Acoustical Society of America. 2014;135: 2995–3006. doi:10.1121/1.4870486

75. Hämäläinen MS. Functional localization based on measurements with a whole-head magnetometer system. Brain topography. 1995;7: 283–9. doi:10.1007/BF01195254

76. Taulu S, Simola J, Kajola M. Applications of the signal space separation method. IEEE Transactions on Signal Processing. 2005;53: 3359–3372. doi:10.1109/TSP.2005.853302

77. Hebart MN, Görgen K, Haynes J-D. The Decoding Toolbox (TDT): a versatile software package for multivariate analyses of functional imaging data. Frontiers in Neuroinformatics. 2015;8. Available: https://www.frontiersin.org/articles/10.3389/fninf.2014.00088

78. Maris E, Oostenveld R. Nonparametric statistical testing of EEG- and MEG-data. Journal of neuroscience methods. 2007;164: 177–90. doi:10.1016/j.jneumeth.2007.03.024

79. Kriegeskorte N, Goebel R, Bandettini P. Information-based functional brain mapping. Proceedings of the National Academy of Sciences of the United States of America. 2006;103: 3863–3868. doi:10.1073/pnas.0600244103

80. Walther A, Nili H, Ejaz N, Alink A, Kriegeskorte N, Diedrichsen J. Reliability of dissimilarity measures for multi-voxel pattern analysis. NeuroImage. 2016;137: 188–200. doi:10.1016/j.neuroimage.2015.12.012

Figure 1

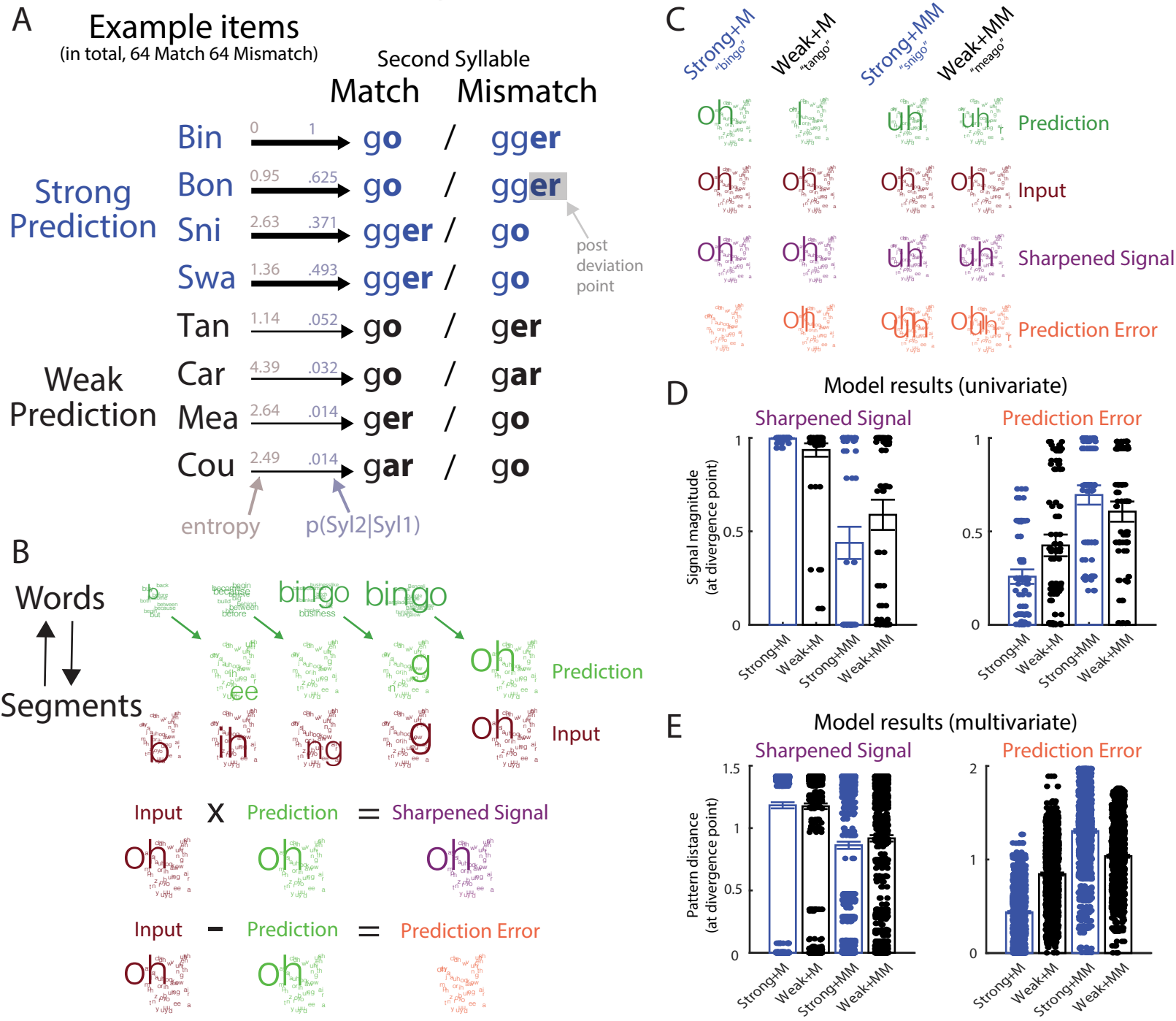
A
Example items
(in total, 64 Match 64 Mismatch)
Second Syllable
Match
Mismatch
Strong Prediction
Weak Prediction
Bin 0 1 go / gger
Bon 0.95 .625 go / gger
Sni 2.63 .371 gger / go
Swa 1.36 .493 gger / go
Tan 1.14 .052 go / ger
Car 4.39 .032 go / gar
Mea 2.64 .014 ger / go
Cou 2.49 .014 gar / go
post deviation point
entropy
p(Syl2|Syl1)
B
Words
Segments
bingo
Prediction
Input
Input X Prediction = Sharpened Signal
Input - Prediction = Prediction Error
C
Strong+M "bingo"
Weak+M "tango"
Strong+MM "snigo"
Weak+MM "meago"
Prediction
Input
Sharpened Signal
Prediction Error
D
Model results (univariate)
Sharpened Signal
Prediction Error
Signal magnitude (at divergence point)
Strong+M
Weak+M
Strong+MM
Weak+MM
E
Model results (multivariate)
Sharpened Signal
Prediction Error
Pattern distance (at divergence point)

Figure 2

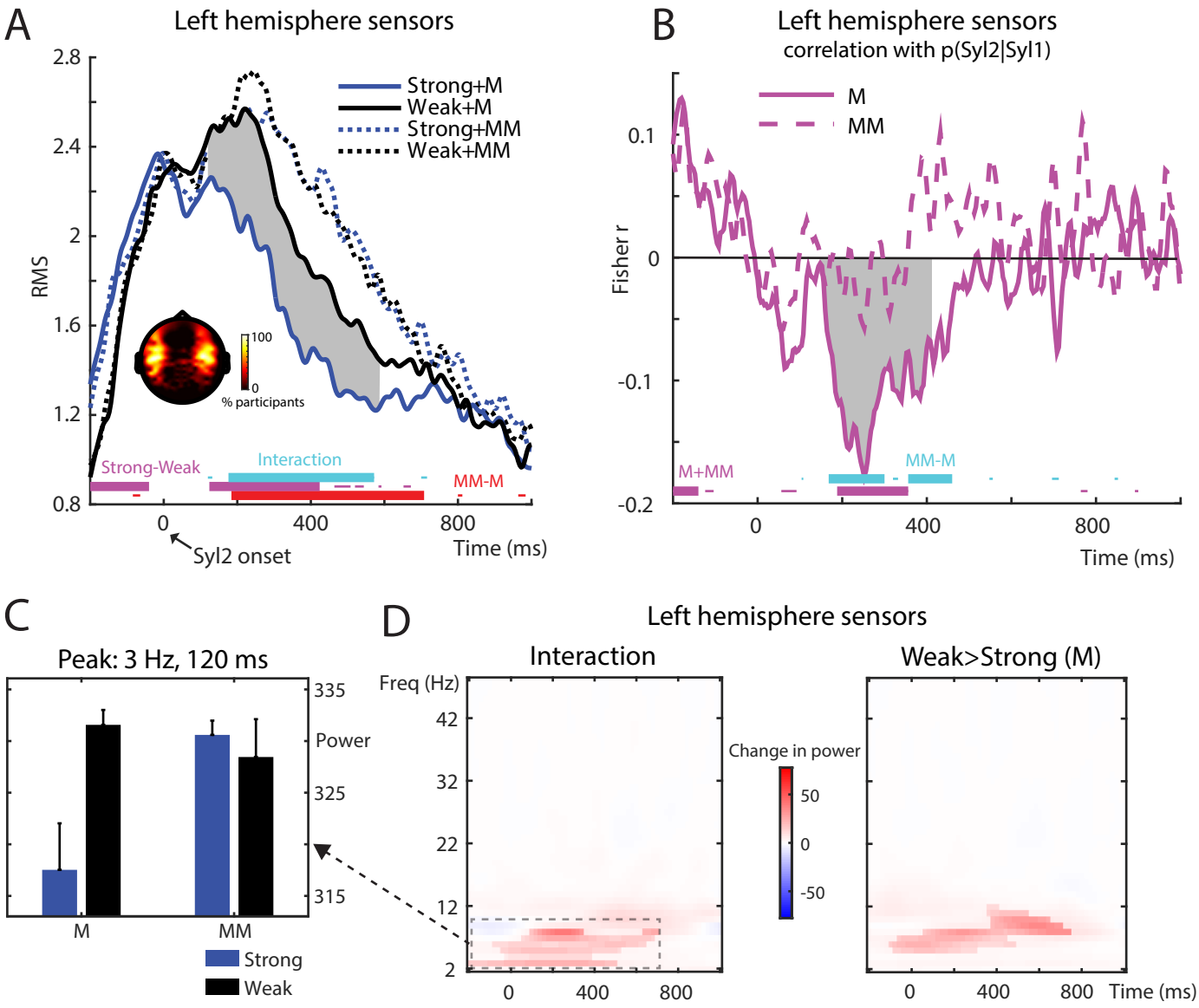
A
Left hemisphere sensors
RMS
2.8
2.4
2
1.6
1.2
0.8
Strong+M
Weak+M
Strong+MM
Weak+MM
100
0
% participants
Strong-Weak
Interaction
MM-M
0
400
800
Syl2 onset
Time (ms)
B
Left hemisphere sensors
correlation with p(Syl2|Syl1)
M
MM
Fisher r
0.1
0
-0.1
-0.2
M+MM
MM-M
0
400
800
Time (ms)
C
Peak: 3 Hz, 120 ms
335
Power
325
315
M
MM
Strong
Weak
D
Left hemisphere sensors
Interaction
Weak>Strong (M)
Freq (Hz)
42
32
22
12
2
Change in power
50
0
-50
0
400
800
Time (ms)

Figure 3

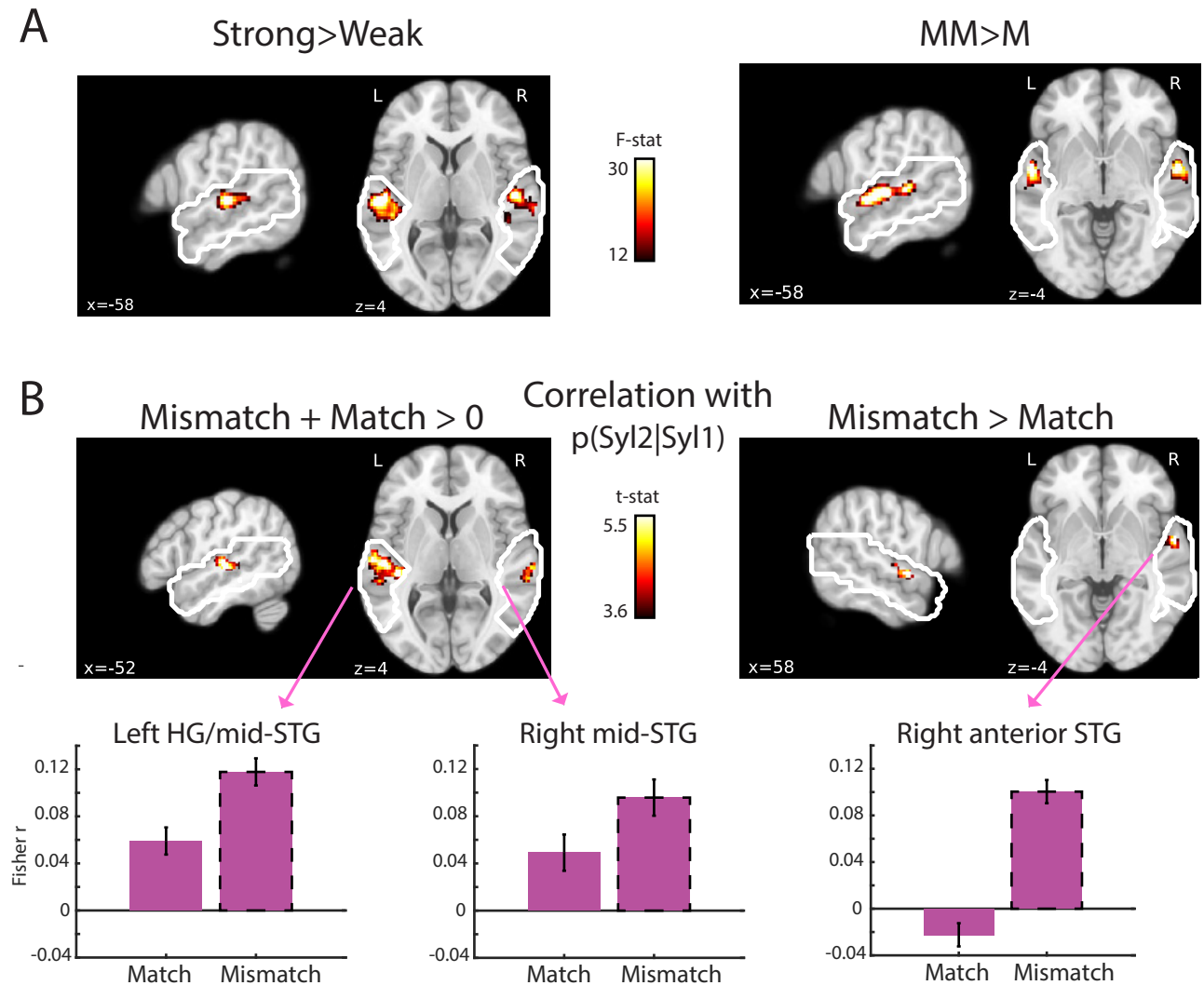
A
Strong>Weak
MM>M
L
R
x=-58
z=4
F-stat
30
12
x=-58
z=-4
B
Mismatch + Match > 0
Correlation with
p(Syl2|Syl1)
Mismatch > Match
t-stat
5.5
3.6
x=-52
z=4
x=58
z=-4
Left HG/mid-STG
Right mid-STG
Right anterior STG
Fisher r
0.12
0.08
0.04
0
-0.04
Match
Mismatch

Figure 4

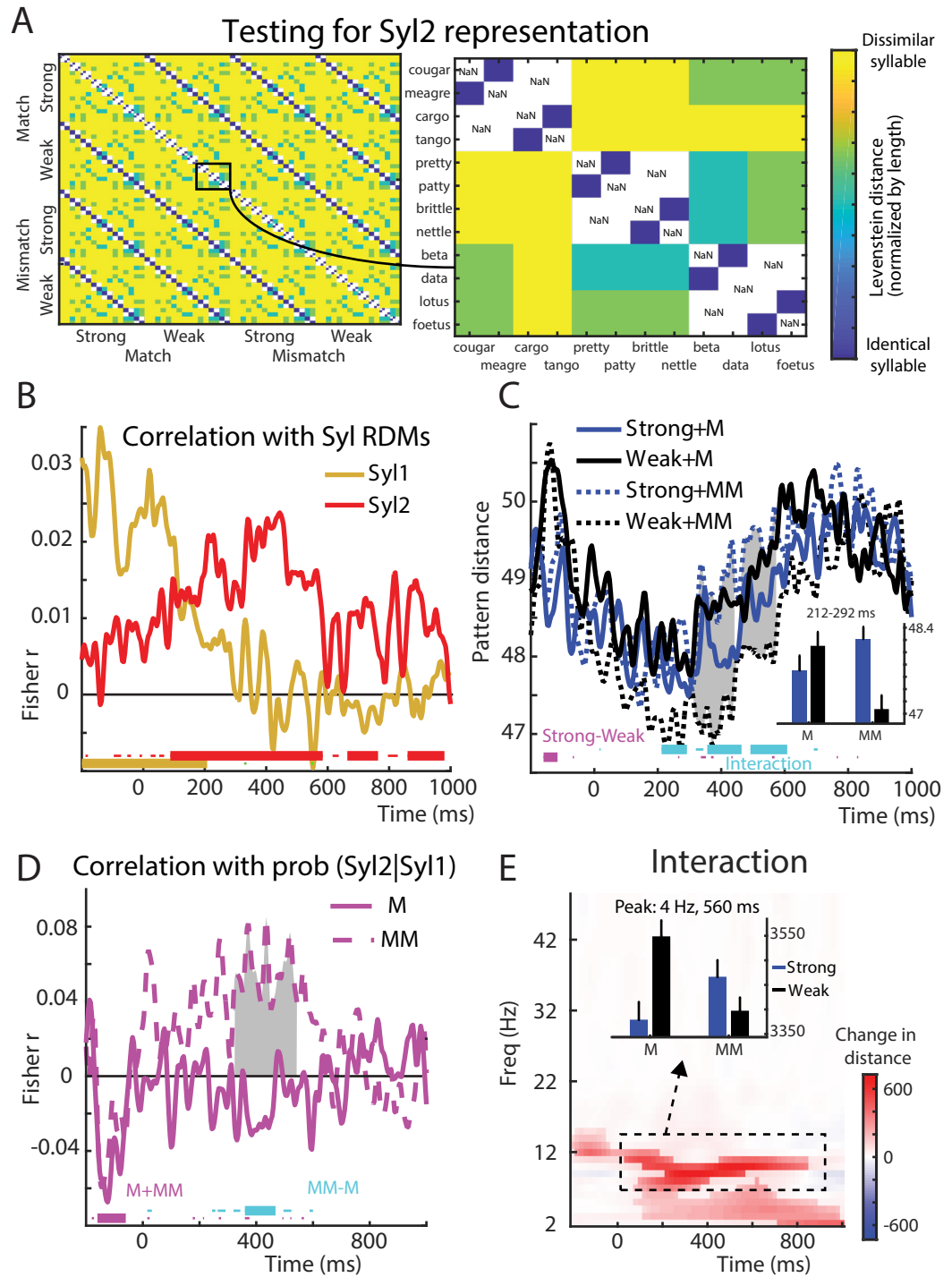
A
Testing for Syl2 representation
Match
Strong
Weak
Mismatch
Strong
Weak
Strong
Weak
Strong
Weak
Match
Mismatch
cougar
meagre
cargo
tango
pretty
patty
brittle
nettle
beta
data
lotus
foetus
NaN
Dissimilar syllable
Levenstein distance (normalized by length)
Identical syllable
B
Correlation with Syl RDMs
Syl1
Syl2
Fisher r
0.03
0.02
0.01
0
0
200
400
600
800
1000
Time (ms)
C
Strong+M
Weak+M
Strong+MM
Weak+MM
Pattern distance
50
49
48
47
212-292 ms
48.4
47
M
MM
Strong-Weak
Interaction
0
200
400
600
800
1000
Time (ms)
D
Correlation with prob (Syl2|Syl1)
M
MM
Fisher r
0.08
0.04
0
-0.04
M+MM
MM-M
0
400
800
Time (ms)
E
Interaction
Peak: 4 Hz, 560 ms
3550
3350
Strong
Weak
M
MM
Freq (Hz)
42
32
22
12
2
Change in distance
600
0
-600
0
400
800
Time (ms)

Figure 5

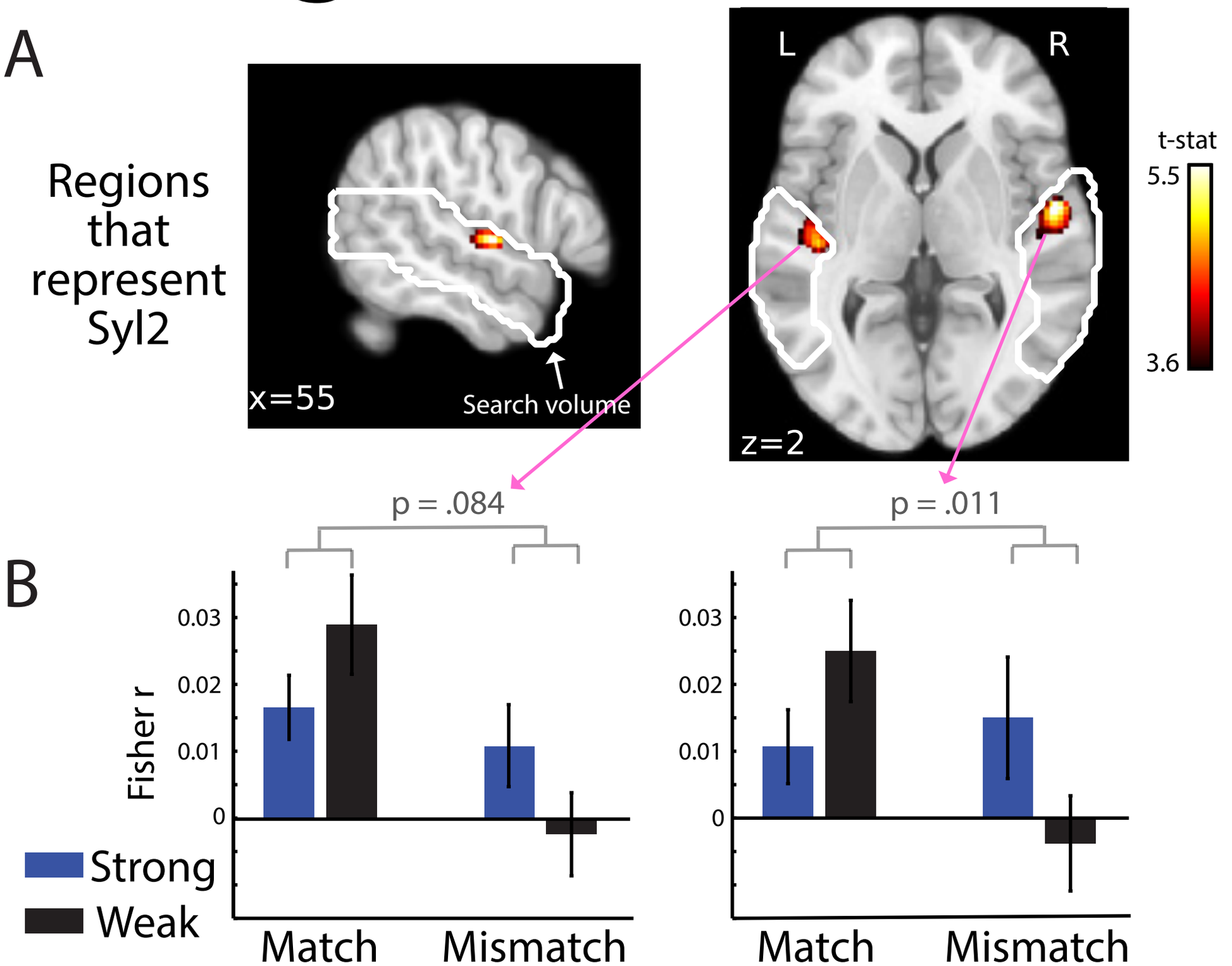
A
Regions that represent Syl2
x=55
Search volume
L
R
z=2
t-stat
5.5
3.6
B
p = .084
p = .011
Fisher r
0.03
0.02
0.01
0
Strong
Weak
Match
Mismatch
Match
Mismatch
Interaction (both hemispheres): p = .005

Figure 6

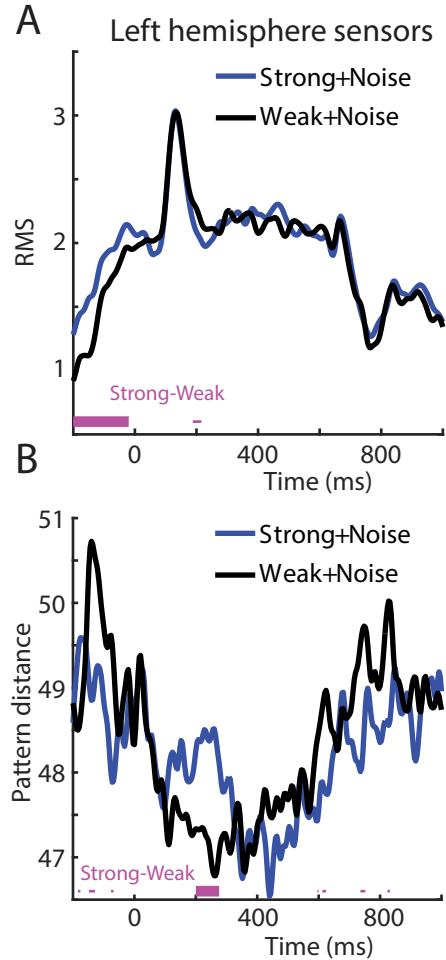
A
Left hemisphere sensors
Strong+Noise
Weak+Noise
RMS
3
2
1
Strong-Weak
0
400
800
Time (ms)
B
Strong+Noise
Weak+Noise
Pattern distance
51
50
49
48
47
Strong-Weak
0
400
800
Time (ms)

Table 1

Location	Extent	Z-stat	x	y	z
Univariate Strong > Weak					
Right Heschl's Gyrus	551	5.74	54	-16	2
Right mid-STG		4.84	64	-14	0
Right mid-STG		4.05	66	-26	4
Left mid-STG	551	5.41	-58	-22	4
Left Heschl's Gyrus		4.55	-44	-24	2
Left mid-STG		4.55	-46	-32	4
Univariate Mismatch > Match					
Left mid-STG	569	6.00	-64	-24	6
Left mid-STG		5.81	-60	-16	2
Left anterior-STG		5.62	-58	-4	-4
Right anterior-STG	205	5.25	58	-4	-4
Right mid-STG		4.51	64	-16	0
Right mid-STG		3.54	56	-14	-2
Univariate Strong+Noise > Weak+Noise					
Left anterior-STG	245	4.42	-54	-12	2
Left Heschl's Gyrus		4.21	-44	-22	-2
Left mid-STG		3.31	-60	-24	2
Right posterior-STG	56	4.25	64	-44	10
Right posterior-MTG		3.58	60	-54	6
Right mid-STG	115	4.00	54	-20	0
Right Heschl's Gyrus		3.30	48	-14	0
Right anterior-STG		3.10	58	-12	-4
Univariate correlations with p(Syl2|Syl1) Mismatch+Match					
Left Heschl's Gyrus	467	5.01	-52	-22	2
Left Heschl's Gyrus		4.85	-42	-28	4
Left mid-STG		4.62	-62	-18	6
Right mid-STG	105	4.04	66	-24	6
Right mid-STG		3.96	64	-32	6
Right mid-STG		3.56	54	-26	0
Univariate correlations with p(Syl2|Syl1) Mismatch>Match					
Right anterior-STG	71	4.58	58	-2	-4
Right anterior-STG		3.81	50	-4	-2
Right anterior-STG		3.59	58	-10	2
Multivariate Syl2 phonetic distance					
Right Heschl's Gyrus	148	4.49	56	-6	2
Left Heschl's Gyrus	146	4.01	-44	-20	0

SI Methods

Web-based gating study

Our measure of p(Syl2|Syl1) is derived from frequency counts and phonological transcriptions in the CELEX database [66]. To validate this measure, we conducted a web-based gating task [23] using the Strong+Noise and Weak+Noise stimuli (each item presented once in a random order). Participants were British English speakers (N=110, recruited via https://www.prolific.co), aged 18 to 40 years and self-reported having no hearing difficulties or language-related disorders. They were told that they would hear real English words “partly hidden by noise” and asked to report the identity of the word by typing it out. For each item, we calculated the proportion of participants reporting the source word i.e. the matching word prior to replacing Syl2 with noise.

Cued recall task

After the fMRI scans, listeners completed a cued recall test assessing memory for the pseudowords. Data were not available for this task for four participants either because of technical issues or because the participant did not understand the task instructions. The final sample size consisted of 17 participants for this test. We cued participants with the first syllable of each pseudoword item by presenting the Strong+Noise and Weak+Noise items. Participants were told that the nonsense (pseudo) words were “partly hidden by noise” and were asked to recall the nonsense word by saying it aloud. Responses were scored for accuracy based on counting the percentage of trials in which participants generated the correct Syl2 used in the Mismatch items.

SI Results

Stimulus properties

A summary of stimulus properties is shown in Figure S4A and S4B. Based on frequency counts, and phonological transcriptions in CELEX, the average conditional

probability of syllable 2 given syllable 1 (p(Syl2|Syl1)) for Strong prediction items was 0.574 (SD = 0.332) while for Weak items it was 0.019 (SD = 0.029). Strong items were also associated with smaller syllable entropy (calculated as the negative sum of log-transformed p(Syl2|Syl1) over all possible syllables; mean = 1.34, SD = 1.11) than Weak items (mean = 2.99, SD = 0.99). Strong and Weak items had similar log frequencies (Strong: mean = 4.90, SD = 1.56; Weak: mean = 3.89, SD = 1.62) although the difference was significant (independent samples $t(62) = 2.53$, $p = 0.014$). However, all reported MEG and fMRI effects involving correlations with conditional probabilities (Figures 2B, 3B and 4D) survive when controlling for differences in word frequency (using partial Spearman correlations). Moreover, p(Syl2|Syl1) is the strongest predictor of listeners' behaviour in a free report gating task (conducted in a separate group of listeners; see Figure S1E and SI Methods for more details), as compared with word frequency and syllable entropy. Thus, we are confident that our effects of prediction strength after Syl2 onset stem from differences in conditional probability rather than differences in word frequency.

For the fMRI experiment (Figure S4A), the Syl1 portion of Strong items was lower in acoustic intensity ($t(62) = -2.14$, $p = 0.036$) and longer in duration ($t(62) = 3.47$, $p < .001$) than Weak items. The RMS intensity for Syl1 and Syl2 was separately normalised over items for the MEG experiment (which was conducted after the fMRI experiment) and did not differ between conditions (Figure S4B). All other stimulus properties did not differ between the fMRI and MEG experiments. Importantly, there were no acoustic differences between conditions for the Syl2 portion of our stimuli. Neural responses to Syl2 are the key focus of this study since it is representations of Syl2 that distinguish sharpened signal and prediction error accounts.

Web-based gating study

Listeners were told that they would hear real English words "partly hidden by noise" and asked to report the identity of the word by typing it out (see SI Methods). p(Syl2|Syl1) was strongly correlated with the probability of listeners' responses ($r(108) = .636$, $p < .001$; see Figure S1E). That is, more strongly predicted second syllables were more likely to be reported by listeners, confirming that our experimental manipulation of prediction strength was successful.

Cued recall task

After the fMRI scans, we assessed listeners' memory for the pseudowords in a cued recall task (see SI Methods). We cued participants with the first syllable of each pseudoword item by presenting the Strong+Noise and Weak+Noise items. Participants were told that the nonsense (pseudo) words were "partly hidden by noise" and were asked to recall the nonsense word by saying it aloud. Recall accuracy (percentage correct) was around 10% on average over participants, with most participants achieving 5% or higher (see Figure S1D). These data indicate the recall task was difficult. Importantly however, they also suggest that participants could perform the task to some degree and hence were attentively processing the pseudoword stimuli. Recall accuracy was better for pseudowords formed with Strongly- versus Weakly-predicting first syllables (one-tailed $t(16) = 1.768$, $p = .048$), consistent with the proposal that items evoking strong prediction errors are learned more readily than items evoking weak prediction errors [see ref. 3 and Discussion].

Supplementary figure captions

Figure S1- Method and behavioural results. (A) Participants listened to the spoken stimuli and detected a brief pause that appeared occasionally between Syl1 and Syl2 by responding with a button press. MEG and fMRI were recorded in two separate groups of participants (N = sample size for each group). Two example trials are indicated with stimulus and scan timings. TA = time of fMRI scan acquisition. TR = repetition time for fMRI scans. SOA = Stimulus Onset Asynchrony. s = seconds. ms = milliseconds. (B) Bar graph showing group-averaged d-primes and response times (target-present trials) for the pause detection task in the MEG experiment (with within-subject standard errors). Individual lines represent individual participants. (C) Same as panel B but for pause detection responses in the fMRI experiment. (D) Percentage correct accuracy of pseudoword memory in a cued recall test conducted after the fMRI scans. For this recall test, participants were presented with the Strong+Noise and Weak+Noise items and asked to recall previously heard pseudowords that started with the same first syllable. (E) Scatter plots of the percentage of participants identifying items in a web-based gating pre-test study against p(Syl2|Syl1), entropy and word frequency (each circle representing one of the 64 word items used in the experiment). Correlation coefficients (and p values) for each relationship are shown above each graph with further partial correlations reported within brackets.

Figure S2- Supplementary MEG analyses. (A) Same as Figure 2A but for right hemisphere sensors. (B) Same as Figure 2B but for right hemisphere sensors. (C) Same as Figure 2B for MEG signal timelocked to Syl1 onset. (D) Pattern analysis showing simple effect of Weak > Strong (Match) on MEG pattern distances.

Figure S3- Same as Figure 1C and 1D but showing the impact of varying sensory uncertainty levels (using the Softmax Temperature parameter) for Sharpened Signal (upper panels) simulations and Prediction Error (lower panels) for simulations of (A) Signal magnitude and (B) Pattern distance results. To give an indication of the degree of sensory uncertainty for each simulation, above each graph we show the average along the diagonal of the acoustic similarity matrix used for modelling the

sensory evidence. This quantity can be interpreted as the average probability of correctly identifying speech segments. The simulation results depicted in Figure 1C and 1D correspond to the graphs in the second column (i.e. Evidence = 0.78).

Figure S4- (A) Stimulus properties for the fMRI experiment (means and standard errors of the mean). (B) The RMS intensity of the stimuli for the MEG experiment, which were slightly different to those for the fMRI experiment (all other stimulus properties did not differ) (C) Histograms showing the distribution of item durations in our stimuli as well as Syl1 and Syl2 durations.

Figure S5- Same as Figure 4A. Phonetic dissimilarity matrix expressing the normalized Levenshtein distance between phonetic transcriptions of Syl1 in different items.

Figure S1

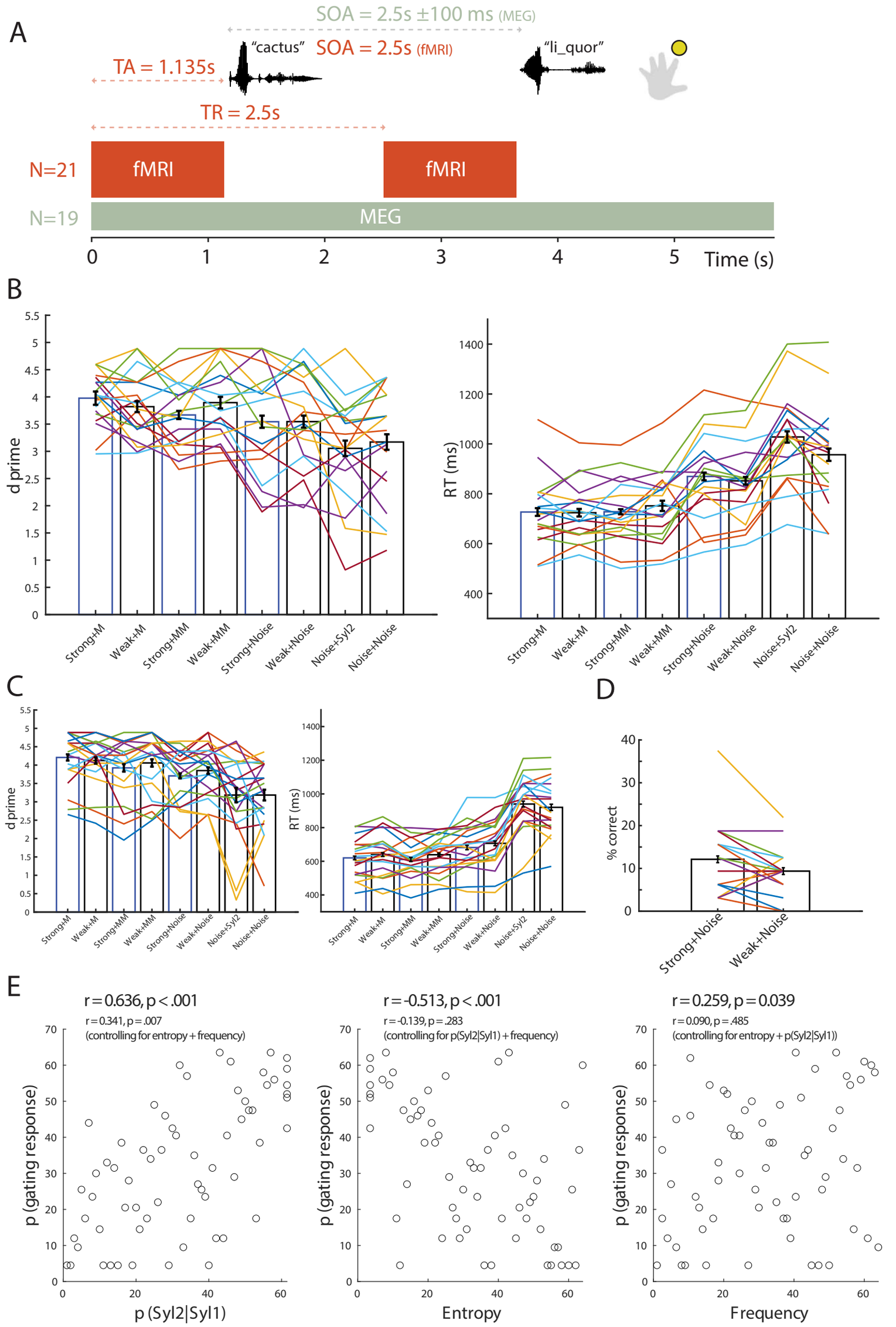
A
SOA = 2.5s ±100 ms (MEG)
"cactus"
SOA = 2.5s (fMRI)
"li_quor"
TA = 1.135s
TR = 2.5s
N=21
fMRI
fMRI
N=19
MEG
0
1
2
3
4
5
Time (s)
B
d prime
RT (ms)
Strong+M
Weak+M
Strong+MM
Weak+MM
Strong+Noise
Weak+Noise
Noise+Syl2
Noise+Noise
C
d prime
RT (ms)
D
% correct
Strong+Noise
Weak+Noise
E
r = 0.636, p < .001
r = 0.341, p = .007
(controlling for entropy + frequency)
p (gating response)
p (Syl2|Syl1)
r = -0.513, p < .001
r = -0.139, p = .283
(controlling for p(Syl2|Syl1) + frequency)
Entropy
r = 0.259, p = 0.039
r = 0.090, p = .485
(controlling for entropy + p(Syl2|Syl1))
Frequency

Figure S2

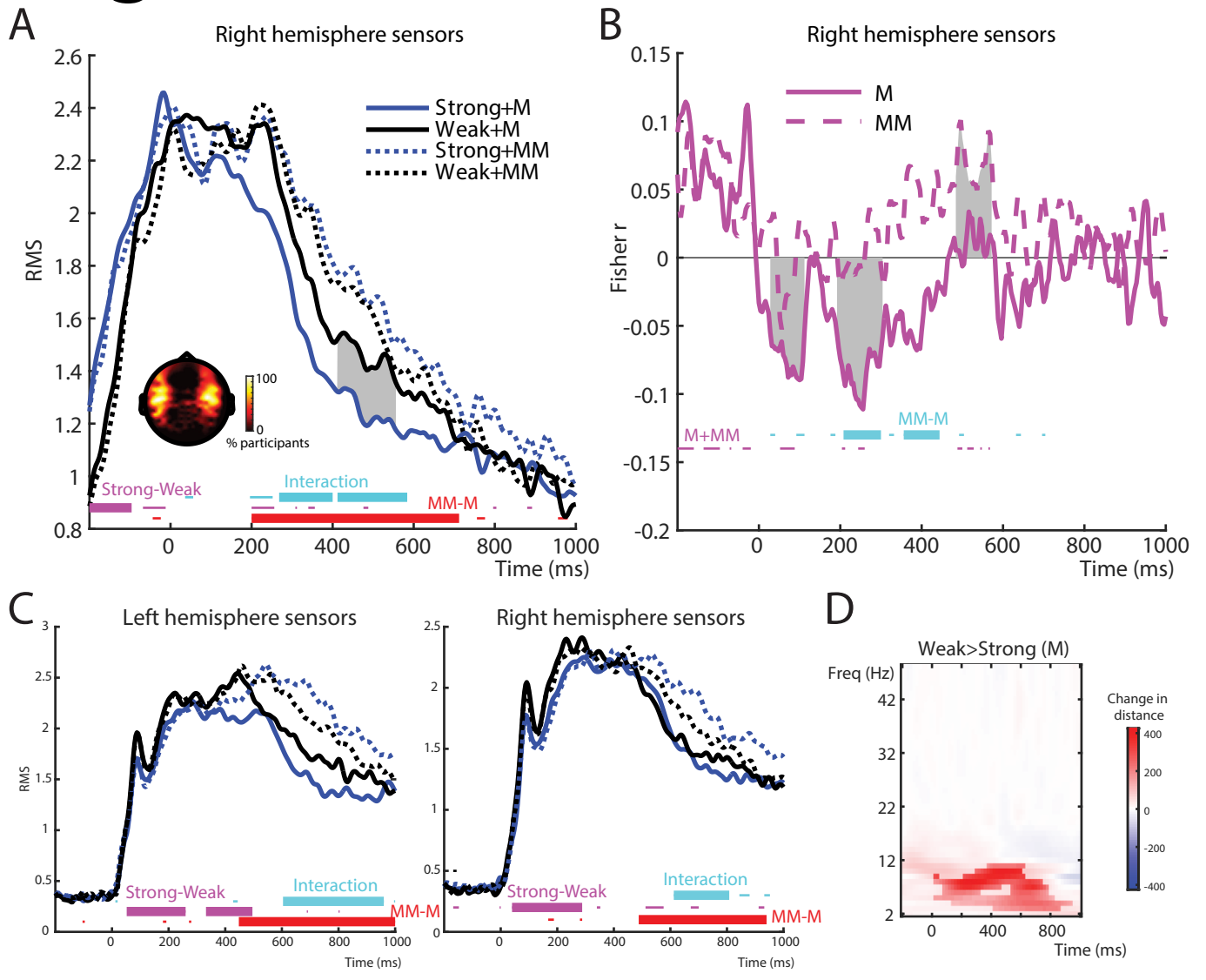
A
Right hemisphere sensors
RMS
Time (ms)
Strong+M
Weak+M
Strong+MM
Weak+MM
100
0
% participants
Strong-Weak
Interaction
MM-M
B
Right hemisphere sensors
Fisher r
Time (ms)
M
MM
M+MM
MM-M
C
Left hemisphere sensors
Right hemisphere sensors
RMS
Time (ms)
Strong-Weak
Interaction
MM-M
D
Weak>Strong (M)
Freq (Hz)
Time (ms)
Change in distance

Figure S3

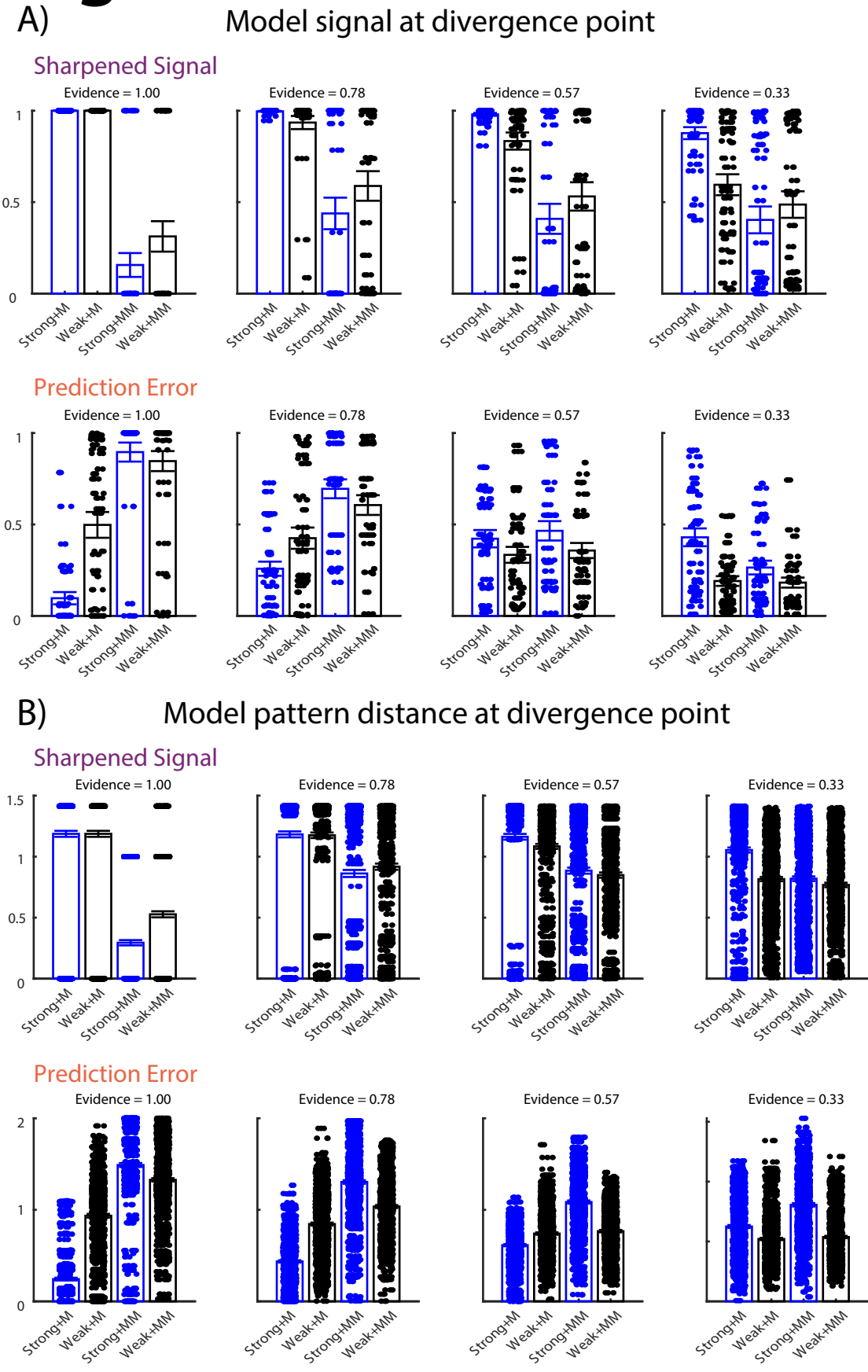
A)
Model signal at divergence point
Sharpened Signal
Evidence = 1.00
Evidence = 0.78
Evidence = 0.57
Evidence = 0.33
Prediction Error
B)
Model pattern distance at divergence point
Sharpened Signal
Prediction Error
Strong+M
Weak+M
Strong+MM
Weak+MM

Figure S4

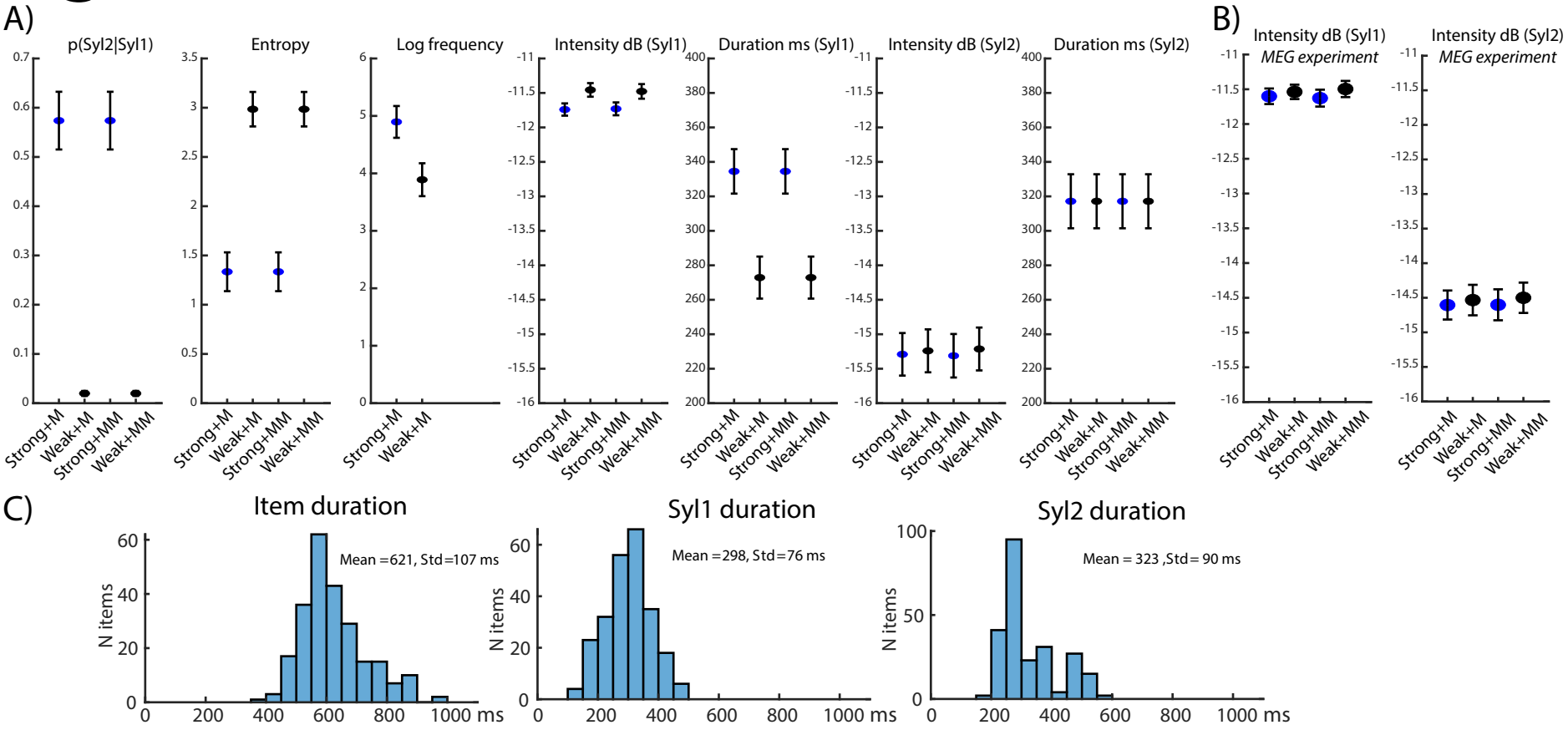
A)
p(Syl2|Syl1)
Entropy
Log frequency
Intensity dB (Syl1)
Duration ms (Syl1)
Intensity dB (Syl2)
Duration ms (Syl2)
Strong+M
Weak+M
Strong+MM
Weak+MM
B)
Intensity dB (Syl1)
MEG experiment
Intensity dB (Syl2)
MEG experiment
C)
Item duration
Mean =621, Std=107 ms
Syl1 duration
Mean =298, Std=76 ms
Syl2 duration
Mean = 323 ,Std= 90 ms
N items
ms

Figure S5

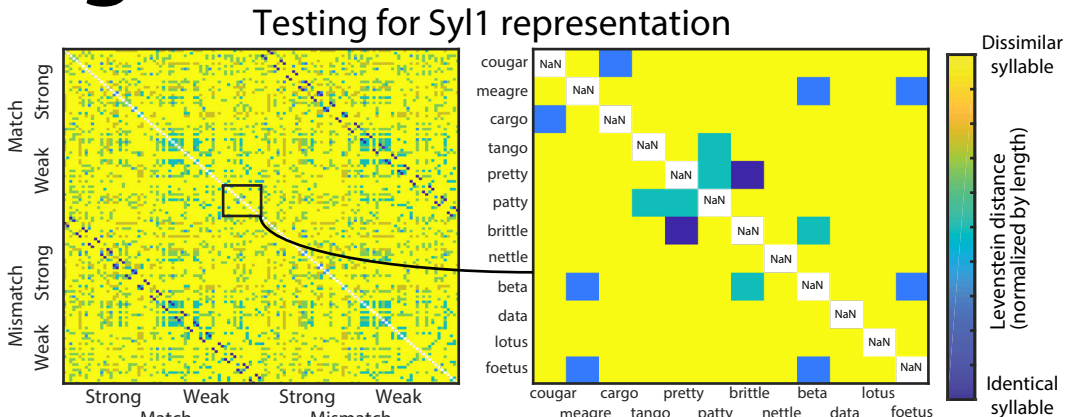
Testing for Syl1 representation
Match
Strong
Weak
Mismatch
Strong
Weak
Strong
Weak
Match
Strong
Weak
Mismatch
cougar
meagre
cargo
tango
pretty
patty
brittle
nettle
beta
data
lotus
foetus
NaN
Dissimilar syllable
Levenstein distance (normalized by length)
Identical syllable